Title

A hidden Markov model approach for simultaneously estimating local ancestry and admixture time using next generation sequence data in samples of arbitrary ploidy

Short Title

Estimating local ancestry and admixture time in samples of arbitrary ploidy

Authors

Russell Corbett-Detig[1,2,*] and Rasmus Nielsen[2,3]

[1]Department of Biomolecular Engineering, UC Santa Cruz, Santa Cruz, CA
[2]Department of Integrative Biology, UC Berkeley, Berkeley, CA
[3]The Natural History Museum of Denmark, University of Copenhagen, Denmark.
*Correspondence to: russcd@gmail.com

Keywords

Local Ancestry Inference, Admixture, Hidden Markov Model, *Drosophila melanogaster*, Pool-seq

Abstract

Admixture—the mixing of genomes from divergent populations—is increasingly appreciated as a central process in evolution. To characterize and quantify patterns of admixture across the genome, a number of methods have been developed for local ancestry inference. However, existing approaches have a number of shortcomings. First, all local ancestry inference methods require some prior assumption about the expected ancestry tract lengths. Second, existing methods generally require diploid genotypes, which is not feasible to obtain for many sequencing projects. Third, many methods assume samples are diploid, however a wide variety of sequencing applications will fail to meet this assumption. To address these issues, we introduce a novel hidden Markov model for estimating local ancestry that models the read pileup data, rather than genotypes, is generalized to arbitrary ploidy, and can estimate the time since admixture during local ancestry inference. We demonstrate that our method can simultaneously estimate the time since admixture and local ancestry with good accuracy, and that it performs well on samples of high ploidy—*i.e.* 100 or more chromosomes. We apply our method to pooled sequencing data derived from populations of *Drosophila melanogaster* on an ancestry cline on the east coast of North America. We find that regions of low recombination show steeper clines than regions of high recombination, suggesting that selection against foreign ancestry has had the largest effect in these regions presumably due to increased linkage between neutral and selected sites. We also identify numerous outlier loci associated with behavior suggesting selection associated with prezygotic reproductive isolation. Finally, we identify candidate genes associated with reproductive isolation between ancestral

47 subpopulations of *D. melanogaster*. Our results illustrate the potential of local ancestry
48 inference for elucidating fundamental evolutionary processes.
49
50 **Author Summary**
51 When divergent populations hybridize their offspring obtain a portion of their genome
52 from each parent population. Although the average ancestry proportion in each descendant
53 is equal to the proportion of ancestors from each of the ancestral populations, the
54 contribution of each ancestry type is variable across the genome. Estimating local ancestry
55 within admixed individuals is a fundamental goal for evolutionary genetics, and here we
56 develop a method for doing this that circumvents many of the problems associated with
57 existing methods. Briefly, our method can use short read data, rather than genotypes and
58 can be applied to samples with any number of chromosomes. Furthermore, our method
59 simultaneously estimates local ancestry, and the number of generations since admixture—
60 the time that the two ancestral populations first encountered each other. Finally, in
61 applying our method to data from an admixture zone between ancestral populations of
62 *Drosophila melanogaster*, we find many lines of evidence consistent with natural selection
63 operating to against the introduction of foreign ancestry into populations of predominantly
64 one ancestry type. Because of the generality of this method, we expect that it will be useful
65 for a wide variety of existing and ongoing research projects.
66

Introduction

Characterizing the biological consequences of admixture—the mixing of genomes from divergent ancestral populations—is a fundamental and important challenge in evolutionary genetics. Admixture has been reported in a variety of natural populations of animals [1,2], plants [3-5] and humans [6,7], and theoretical and empirical evidence suggests that admixture may affect a diverse suit of evolutionary processes. Individuals' ancestry can affect disease susceptibility in admixed populations, and inferring and correcting for sample population ancestries is a common practice in human genome wide association studies [8-10]. More generally, admixture has the potential to influence patterns of genetic variation within populations [11,12], to introduce novel adaptive [13,14] and deleterious variants [7,15,16], as well as to disrupt epistatic gene networks [17,18]. Therefore, developing a comprehensive understanding of the extent of admixture in natural populations and resulting mosaic genome structures is essential to furthering our understanding of a diverse suite of evolutionary processes.

Estimating genome-wide ancestry proportions has become a common practice in population genetic inference. For example, the program STRUCTURE [19], originally released in 2000, uses a Bayesian framework to model the ancestry proportions of individuals derived from any number of source populations based on genotype data at a set of unlinked genetic markers. More recently, this model for ancestry proportion estimation has been extended to cases where individual genotypes are not known, but can be studied probabilistically using low-coverage sequencing short read sequencing data [20], which is an important step towards accommodating modern sequencing practices. Additionally,

Bergland *et. al.* [21] developed a method for estimating ancestry proportions in pooled population samples of relatively high ploidy (*i.e.* 40-250 distinct chromosomes) from short read sequencing data. In general, it is straightforward to estimate genome-wide ancestry proportions using a number of sequencing strategies and applications.

It is substantially more challenging to accurately estimate local ancestry (LA) at markers distributed along the genome of a sample. Nonetheless, analyses of LA have the potential to yield more nuanced insights into our understanding of the evolutionary processes affecting ancestry proportions across the genome. One of the first LAI methods was an extension of the STRUCTURE [19] framework that modeled the correlation in ancestry among markers due to linkage. Because the ancestry at each locus is not observed, Falush *et al.* [22] suggested that a hidden Markov model is a straightforward means of inferring the ancestry states at each site in the genome (which are unobserved) based on observed genotype data distributed along a chromosome. Most subsequent LAI methods have also used an HMM framework. The majority of LAI models that have been developed are geared towards estimating LA in admixed human populations (*e.g.* [23,24]). Consequently, most existing LAI methods are limited to diploid genomes with high quality genotype calls. Furthermore, many methods require phased reference panels [24,25], and require the user to provide an estimate of, or make implicit assumptions about, the number of generations since the initial admixture event [2,23-25]. This is straightforward with human population genomic samples, where abundant high quality genotyped samples are available and for which well-documented demographic histories are sometimes known. However for most other species,

112 demographic histories are less well characterized, and assumptions about admixture times
113 may bias the result of LAI methods.
114
115 A number of approaches exist to estimate the time since admixture based on a well
116 characterized ancestry tract length distributions [26-29] but in general, these parameters
117 are unknown prior to LAI. We may therefore expect to improve LAI by simultaneously
118 estimating LA and demographic parameters (*e.g.* admixture time). Furthermore, in the
119 majority of sequencing applications, relatively low individual sequencing coverage is often
120 used to probabilistically estimate individual and population allele frequencies (*e.g.* [30])
121 but these data are often not sufficient to determine high confidence genotypes that are
122 required for existing LAI applications. Hence, there is a clear need for a general LAI method
123 that can accommodate genotype uncertainty and requires less advanced knowledge of
124 admixed populations' demographic histories.
125
126 Here, we introduce a framework for simultaneously estimating LA using short read pileup
127 data and the time of admixture within a population. Briefly, as with many previously
128 proposed LAI methods, we model ancestry across the genome of a sample as a hidden
129 Markov model (HMM). We estimate LA by explicitly modeling read counts as a function of
130 sample allele frequencies within an admixed population. Our method is generalized to
131 accommodate arbitrary sample ploidies, and is therefore applicable to haploid (or inbred),
132 diploid, tetraploid, as well as pooled sequencing applications. We show that this approach
133 accurately infers the time since admixture when data are simulated under the assumed
134 model. Furthermore, our method yields accurate LA estimates for simulated datasets,

including samples of high sample ploidy and including evolutionary scenarios that violate the assumptions of the neutral demographic model. In comparisons between ours and one existing LAI method, LAMPanc [23], we find that our approach offers a significant improvement and is accurate over longer time scales. Furthermore, we demonstrate, using a published dataset, that even state-of-the-art LAI methods can be significantly impacted by assumptions about the time since admixture, and that our method provides a solution to this problem.

Finally, we apply this method to a *Drosophila melanogaster* ancestry cline on the east coast of North America. This species originated in sub-Saharan Africa, and approximately 10,000—15,000 years ago a subpopulation expanded out of the ancestral range. During this expansion, the derived subpopulation experienced a population bottleneck that resulted in decreased nucleotide polymorphism, extended linkage disequilibrium within the derived population and substantial genetic differentiation between ancestral and derived populations [2,31-35]. Hereafter, the ancestral population will be referred to as "African" and the derived population as "Cosmopolitan". Following this bottleneck, descendant populations of African and Cosmopolitan *D. melanogaster* have admixed in numerous geographic regions [2,11,21]. Of particular relevance to this work, North America was colonized recently by a population descendent from African individuals from the South, and by a population descendent from cosmopolitan *D. melanogaster* in the North [11,21,34]. Where these populations encountered each other in eastern North America, they form an ancestry cline where southern populations have a greater contribution of African ancestry than northern populations [21].

158

159 Previous work on these ancestry clines has shown that ancestry proportions vary across
160 populations with increasing proportions of cosmopolitan alleles in more temperate
161 localities. Evidence suggests spatially varying selection affects the distribution of genetic
162 variants [36-41]. Furthermore, strong epistatic reproductive isolation barriers partially
163 isolate individuals from northern and southern populations along this ancestry cline
164 [42,43]. This may be generally consistent with recent observations of ancestry-associated
165 epistatic fitness interactions within a *D. melanogaster* population in North Carolina [17],
166 and with the observation of widespread fitness epistasis between populations of this
167 species more generally [44]. There is therefore good reason to believe that natural
168 selection has acted to shape LA clines that are tightly linked to selected mutations in these
169 *D. melanogaster* populations.

170

171 Here, we show that the slopes of LA clines in North American *D. melanogaster* are
172 positively correlated with recombination rates, consistent with natural selection acting to
173 reduce African introgression into predominantly Cosmopolitan populations. We also find
174 that the X displays a higher rate of LA outlier loci, potentially consistent with a greater role
175 of the X chromosome in genetically isolating Cosmopolitan and African lineages, and we
176 identify numerous clinal outlier loci. These loci are disproportionately likely to be
177 associated with organismal behavior, and may play important roles in generating and
178 maintaining reproductive isolation between African and Cosmopolitan *D. melanogaster*
179 populations.

180

Results and Discussion

The Model

Although admixed populations often are diploid, we derived a general model of ploidy in which the individual has n gene copies at each locus, i.e. for diploid species $n = 2$. In practice, sequences are often obtained from fully or partially inbred individuals (e.g. [35]), which represent only a single uniquely derived chromosome. It is also common to pool individuals prior to sequencing for allele frequency estimation, so called pool-seq (e.g. [21,36,38,45-48]). If the pooling fractions are exactly equal, such a sample of b diploid individuals can be treated as a sample from a single individual with ploidy $n = 2b$. Although that requirement is restrictive, pool-seq has been experimentally validated as a method for accurate allele frequency estimation—*i.e.* alleles are approximately binomially sampled from the sample allele frequencies [49]. We therefore aimed to derive a model that can accommodate arbitrary sample ploidies. In the model, we assumed that the focal population was founded following a single discrete admixture event between two ancestral subpopulations, labeled 0 and 1, with admixture proportions 1-m and m, respectively, at a time t generations in the past. We modeled emission probabilities such that the method can work directly on read pileup data, rather than high quality known genotypes. Briefly, in our model, we specify an HMM $\{H_v\}$ with state space $S = \{0,1,\ldots,n\}$, where $H_v = i$, $i \in S$, indicates that in the vth position i chromosomes are from population 0 and $n - i$ chromosomes are from population 1. In other words, this HMM enables one to estimate what ancestry frequencies are present at a given site along a chromosome within a sample. Importantly, we designed this method to simultaneously estimate the time of admixture,

204 which is related to the correlation between ancestry informative markers along a
205 chromosome. See Methods for a complete description of the HMM including the emissions
206 and transition probability calculations. The source code and manual are available at
207 https://github.com/russcd/Ancestry_HMM.
208
209 **Dependence on Ancestral Linkage Disequilibrium**
210 Within an admixed population, there are two sources of LD. LD that is induced due to the
211 correlation of alleles from the same ancestry type (*i.e.* admixture LD), and LD that is
212 present within each of the ancestral populations (ancestral LD). Admixture LD, is the signal
213 of LA that we seek to detect using the HMM. The second type, ancestral LD, limits the
214 independence of the ancestral information captured by each marker, and is expected to
215 confound HMM-based analyses, particularly as we aimed to estimate the time since
216 admixture within this framework. We therefore sought to quantify the effect of ancestral
217 LD by discarding one of each pair of sites in LD within either ancestral population. We
218 found that ancestral LD tends to increase admixture time estimates obtained using our
219 method, and we decreased the cutoff of the LD parameter, $|r|$, by 0.1 until the time
220 estimates obtained for single chromosomes were unbiased with respect to the true time
221 since admixture. We found that $|r| \leq 0.4$ fit this criterion, although for relatively ancient
222 admixture events with highly skewed ancestry proportions—*i.e.* $m < 0.1$ or $m > 0.9$—some
223 residual bias was apparent in the estimates of admixture time (Figure 1). This reflects the
224 fact that the SMC' ancestry tract distribution performs poorly with highly skewed ancestry
225 proportions and especially for long times since admixture [50].
226

Figure 1 also reveals a striking difference between otherwise equivalently skewed admixture proportions. For example when $m = 0.1$, there was a much larger effect of ancestral LD than when $m = 0.9$. This is due to differences in the variability and LD within the ancestral populations. That is, due to the strong population bottleneck, cosmopolitan *D. melanogaster* populations have substantially more LD and fewer polymorphic sites than African *D. melanogaster* populations. Because the time estimation procedure appears to be sensitive to the amount of ancestral LD present in the data, simulations of the type we described here may be necessary to determine what $|r|$ cutoffs are required to produce unbiased time estimates given the ancestral LD of the populations in a given analysis using this method.

Accuracy and Applications to Diploid and Pooled Samples

We next sought to quantify the accuracy of our approach across varying sample ploidies and times since admixture (Figure 2). Especially for moderate and short admixture times (*i.e.* 0—500 generations), our method performed well for all ploidies considered and we were able to accurately recover the correct admixture time with relatively little bias. However, as true admixture time increases, the time estimates for pooled samples become significantly less reliable and show a clear negative bias. Nonetheless, across the range of times presented in Figure 2, samples of ploidy one and two showed little bias, and we therefore believe our method will produce sufficiently accurate admixture time estimates for a wide variety of applications.

All measures of accuracy decrease with increasing time since admixture (Figure 2). However, even for relatively long times since admixture—2000 generations—and for large sample ploidies, the mean posterior error remained relatively low for all ancestry proportions and for long times since admixture. This indicates that this approach may be sufficiently accurate for a wide variety of applications, sequencing depths, and sample ploidies. Nonetheless, as the proportion of sites within the 95% credible interval decreased with larger pool sizes, it is clear that for larger pools the posterior credible interval tends to be too narrow, and correcting for this bias may be necessary for applications that are sensitive to the accuracy of the credible interval.

Non-Independence Among Ancestry Tracts

As described above, estimates of the time of admixture demonstrate an apparent bias in pools of higher ploidy (Figure 2). Specifically, time tends to be slightly overestimated for relatively short admixture times and underestimated at relatively long admixture times. This is particularly apparent at highly skewed ancestry proportions. Given that this bias is primarily evident in pools of 10 to 20 individuals, we hypothesized that it might be due to the non-independence of ancestry tracts among chromosomes, which should tend to disproportionately affect samples of higher ploidy because all ancestry breakpoints are assumed to be independent in our model. To test this, we simulated genotype data from independent and identically distributed exponential tract lengths as is assumed by our model. When we ran our HMM on this dataset, we found that no bias is evident for simulations of up to 2000 generations (Figure 3), indicating that the primary cause of this bias was violations in the real data of the independence of ancestry tracts that we assumed

when computing the transition probabilities. However, it should be possible to quantify and correct for this bias in applications of this method that aim to estimate the time since admixture.

Robustness to Unknown Population Size

The transition probabilities of this HMM depend on knowledge of the population size. In practice, this parameter is unlikely to be known with certainty. Hence, to assess the impact of misspecification of the population size, we performed simulations using a range of population sizes that span three orders of magnitude (N=100, 1000, 10000, and 100000). All analyses presented here were conducted by applying our HMM to haploid and diploid samples, but qualitatively similar results hold for samples of larger ploidy (not shown). We then analyzed these data assuming the default population size, 10000, is correct. For relatively short times since admixture, there was not a clear bias for any of the true population sizes considered. However, at longer true admixture times, estimated admixture times for both N=100 and N=1000 asymptote at a number of generations near to the population sizes. This result reflects the fact that smaller populations will tend to coalesce at a portion of the loci in the genome relatively quickly, and ancestry tracts cannot become smaller following coalescence. Nonetheless, the accuracy of LAI remained high even when time estimates were unreliable (Figure 4) for the tested marker densities and patterns of LD. Furthermore, in some cases it should be straightforward to determine if a population has coalesced to either ancestry state at a large portion of the loci in the genome, potentially obviating this issue.

A more subtle departure from the expectation was evident for population sizes that are larger than we assumed in analyzing these data (Figure 4). This likely reflects the fact that the probability of back coalescence to the previous marginal genealogy to the left after a recombination event is inversely related to the population size. Hence, the rate of transition between ancestry types is actually slightly higher in larger populations where back coalescence is less likely than we assumed during the LAI procedure. This produced a slight upward bias in the estimates of admixture time when the population was assumed to be smaller than it is in reality. However, this bias appears to be relatively minor, and we expect that time estimates obtained using this method will be useful so long as population sizes can be approximated to within an order of magnitude. Of course, this bias is not unique to our application, and it will affect methods that aim to estimate admixture time after LAI as well. That is, estimating the correct effective population size is an inherent problem for all admixture demographic inference methods.

Application to Ancient Admixture

Although it is clear that accurately estimating relatively ancient admixture times is challenging in higher ploidy samples, we sought to determine the limits of our approach for LAI and time estimation for longer admixture times for haploid sequence data. Because of rapid coalescence in smaller samples (see above), we performed admixture simulations with a diploid effective population size of 100,000. It is clear that there is a limit to the inferences that can be made directly using our method. Like the higher ploidy samples, time estimates for haploid samples departed from expectations shortly after 2,000 generations since admixture (Figure 5). Nonetheless, the magnitude of this bias is slight,

and it is likely that it could be corrected for when applying this method even for very ancient admixture events. For all admixture times considered, LAI remained acceptably accurate despite the slight bias in time estimates (Figure 5).

Reference Panel Size

One question is what effect varying the reference panel sizes will have on LAI inference using this method. We therefore compared results from reference panels of size 10 with those from panels of size 100 (Figure 6). As with results obtained for reference panels of size 50, panels of size 100 were sufficient to accurately estimate admixture time and LA over many generations since admixture. Whereas, when panel sizes were just 10 chromosomes, time estimates were clearly biased and the result was variable across ancestry proportions (Figure 6). However, since there was a strong correlation between true and estimated admixture times even with relatively small panel sizes, it may therefore be possible to infer the correct time by quantifying this bias through simulation and correcting for it. Furthermore, although LAI is clearly less reliable with smaller panels, these results are not altogether discouraging and this approach, in conjunction with modest reference panels may still be effective for some applications.

High Sample Ploidy

In a wide variety of pool-seq applications, samples are pooled in larger groups than we have considered above (*e.g.* [36,45,47]). We are therefore interested in determining how our method will perform on pools of 100 individuals. Towards this, we performed simulations as before, but we designed our parameters to resemble those of the pooled

sequencing data that we analyze in the application of this method below. Specifically, we simulated data with a mean sequencing depth of 25, a time since admixture of 1500 generations, and an ancestry proportion of 0.8. Consistent with results for ploidy 20, we found that time tends to be dramatically underestimated (*i.e.* the mean estimate of admixture time was 680 generations). However, when we provided the time since admixture, our method produced reasonably accurate LAI for these samples. Although the posterior credible interval was again too narrow, the mean posterior error was just 5.4 (or 0.054 if expressed as an ancestry frequency), indicating that this approach can produce LA estimates that are close to their true values for existing sequencing datasets (*e.g.* Figure 7). However, the HMM's run time increases dramatically for higher ploidy samples and higher sequencing depths, a factor that may affect the utility of this program for some analyses. Nonetheless, for more than 36,000 markers, a sample ploidy of 100 and a mean sequencing depth of 25, the average runtime was approximately 42 hours. In contrast, for the same set of parameters, but where individuals are sequenced and analyzed as diploids, the mean runtime was just 8 minutes.

Robustness to Deviations From the Neutral Demographic Model

An important concern is that many biologically plausible admixture models would violate the assumptions of this inference method. In particular, continuous migration and selection acting on alleles from one parental population are two potential causes of deviation from the expected model in the true data. To assess the extent of this potential bias, we performed additional simulations. First, we considered continuous migration at a constant rate that began t generations prior to sampling. In simulations with continuous migration,

364 additional non-recombinant migrants enter the population each generation. Relative to a
365 single pulse admixture model, this indicates that the ancestry tract lengths will tend to be
366 longer than those under a single pulse admixture model in which all individuals entered at
367 time *t*. Indeed, we found that admixture times tended to be underestimated with models of
368 continuous migration. However, the accuracy of LAI remained high across all situations
369 considered here (Table 1), indicating that the LAI aspect of this approach may be robust to
370 alternative demographic models.
371
372 **Table 1.** Parameter estimation and LAI when admixture occurs at a constant rate, rather
373 than in a single pulse.

Admixture Time	Number of Loci	Sample Ploidy	Estimated Time	Proportion in 95% CI	Mean 95% CI Size	Mean Posterior Error	Proportion MLE Correct
100	2	1	96	1.000	0.017	0.005	0.996
		2	98	0.999	0.082	0.022	0.986
		10	105	0.969	1.370	0.457	0.631
		20	93	0.923	2.194	0.856	0.340
	5	1	91	1.000	0.014	0.004	0.997
		2	88	0.999	0.058	0.017	0.988
		10	85	0.942	0.898	0.382	0.662
		20	65	0.949	1.450	0.834	0.302
	10	1	88	1.000	0.014	0.004	0.997
		2	86	0.999	0.060	0.016	0.989
		10	84	0.972	1.049	0.356	0.719
		20	76	0.944	1.887	0.704	0.459
	20	1	79	1.000	0.012	0.004	0.997
		2	74	0.999	0.041	0.013	0.991
		10	65	0.939	0.645	0.305	0.726
		20	53	0.779	1.082	0.704	0.396
500	2	1	521	0.998	0.096	0.027	0.980
		2	518	0.993	0.352	0.096	0.932
		10	595	0.969	2.243	0.735	0.472
		20	486	0.923	3.272	1.184	0.288
	5	1	430	0.998	0.085	0.024	0.983
		2	411	0.993	0.312	0.087	0.938

10	10	287	0.955	1.842	0.639	0.523
	20	227	0.881	2.712	1.093	0.325
	1	341	0.998	0.058	0.018	0.987
	2	303	0.994	0.192	0.059	0.956
	10	177	0.914	1.197	0.511	0.592
	20	140	0.793	1.884	0.992	0.343
20	1	272	0.999	0.040	0.011	0.992
	2	236	0.995	0.142	0.042	0.970
	10	124	0.957	0.974	0.349	0.740
	20	100	0.918	1.607	0.641	0.563

In the second set of simulations, we considered additive selection on alleles that are perfectly correlated with local ancestry in a given region (*i.e.* selected sites with frequencies 0 in population 0 and frequency 1 in population 1), and experience relatively strong selection (selective coefficients were between 0.005 and 0.05). We placed selected sites at 2, 5, 10 and 20 loci distributed randomly across the simulated chromosome, where admixture occurred through a single pulse. Ancestry tracts tend to be longer immediately surrounding selected sites, and we therefore expected admixture time to be underestimated when selection is widespread. When the number of selected loci was small, time estimates were nearly unbiased (Table 2), suggesting that our approach can yield reliable admixture time estimates despite the presence of a small number of selected loci (*i.e.* 2 selected loci on a chromosome arm). However, with more widespread selection on alleles associated with local ancestry, time estimates showed a downward bias that increased with increasing numbers of selected loci. This is likely because selected loci will tend to be associated with longer ancestry tracts due to hitchhiking. However, the accuracy of the LAI remains high for all selection scenarios that we considered here, further

391 indicating that our method can robustly delineate LA, even when the data violate

392 assumptions of the inference method (Table 1,2).

393

394 **Table 2.** Parameter estimation and LAI when a subset of loci experience natural selection

395 in the admixed population.

Admixture Time	Migration Rate	Sample Ploidy	Estimated Time	Proportion in 95% CI	Mean 95% CI Width	Mean Posterior Error	Proportion MLE Correct
100	0.0005	1	53	1.000	0.002	0.001	1.000
		2	49	1.000	0.006	0.002	0.998
		10	129	0.963	0.305	0.168	0.839
		20	98	0.545	0.328	0.661	0.353
	0.001	1	55	1.000	0.004	0.001	0.999
		2	53	1.000	0.013	0.004	0.997
		10	156	0.951	0.558	0.288	0.727
		20	90	0.551	0.719	0.858	0.179
	0.002	1	54	1.000	0.006	0.002	0.999
		2	52	0.999	0.019	0.006	0.996
		10	123	0.949	0.758	0.354	0.671
		20	74	0.679	1.115	0.889	0.176
	0.004	1	43	1.000	0.008	0.002	0.998
		2	54	0.999	0.035	0.010	0.993
		10	91	0.955	1.085	0.443	0.605
		20	75	0.860	1.788	0.889	0.248
500	0.0005	1	254	0.999	0.033	0.010	0.993
		2	250	0.997	0.121	0.036	0.974
		10	331	0.956	1.395	0.528	0.557
		20	333	0.882	2.321	1.018	0.261
	0.001	1	266	0.999	0.049	0.014	0.990
		2	268	0.996	0.198	0.055	0.962
		10	325	0.967	1.887	0.628	0.521
		20	366	0.926	3.049	1.109	0.294
	0.002	1	294	0.999	0.055	0.016	0.989
		2	297	0.996	0.238	0.064	0.956
		10	352	0.977	2.076	0.639	0.542
		20	370	0.951	3.238	1.073	0.336
	0.004	1	346	0.999	0.038	0.010	0.993
		2	350	0.997	0.164	0.042	0.973
		10	403	0.989	1.634	0.455	0.692

	20	462	0.979	2.773	0.833	0.473

396

397

398 **Comparison to LAMPanc**

399 We next compared the results of our method to those of LAMPanc [23]. Because LAMPanc
400 accepts only diploid genotypes, we provided this program diploid genotype data. However,
401 for these comparisons, we still ran our method on simulated read pileups with the mean
402 depth equal to 2. LAMPanc was originally designed for local ancestry inference in very
403 recently admixed populations. As expected, LAMPanc performed acceptably for very short
404 admixture times, but rapidly decreased in performance with increasing time (Figure 8).
405 However, by default, LAMPanc removes sites in strong LD within the admixed samples,
406 which includes ancestral LD, but also admixture LD—the exact signal LAI methods use to
407 identify ancestry tracts.

408

409 We therefore reran LAMPanc, but instead of pruning LD within the admixed population, we
410 removed sites in strong LD within the ancestral populations as described above in our
411 method. With this modification, LAMPanc performs nearly as well as our method, but
412 remains slightly less accurate especially at longer admixture times (Figure 8). This
413 difference presumably reflects the windowed-based approach of LAMPanc. At longer times
414 since admixture a given genomic window may overlap a breakpoint between ancestry
415 tracts. Although the performance is nearly comparable with this modification, we
416 emphasize that our method enables users to estimate the time since admixture, where this
417 must be supplied for LAMPanc, and allows for LAI on read pileups, therefore incorporating

418 genotype uncertainty into the LAI procedure. Indeed our method is more accurate at longer
419 timescales even when supplied with considerably lower quality read data. However
420 LAMPanc supports LAI with multiple ancestral populations, which our method currently
421 does not (but see Conclusions). Furthermore many extensions of LAMP utilize haplotype
422 information, which may be particularly valuable in populations where LD extends across
423 large distances.
424
425 **Assessing Applications to Human Populations**
426 Given the strong interest in studying admixture and local ancestry in human populations
427 (*e.g.* [22-25]), it is useful to ask if our method can be applied to data consistent with
428 admixed populations of humans. Towards that goal, we simulated data similar to what
429 would be observed in admixture between modern European and African lineages and
430 applied our HMM to estimate admixture times and LA. We found that our method can
431 accurately estimate admixture times for relatively short times since admixture, however,
432 substantially more stringent LD pruning in the reference panels is necessary to produce
433 unbiased estimates (Figure 9). This may be expected given that linkage disequilibrium
434 extends across longer distances in human populations than it does in *D. melanogaster*. In
435 other words, the scales of ancestral LD and admixture LD become similar rapidly in
436 admixed human populations. Furthermore, this approach yields accurate time estimates
437 for shorter times since admixture than with genetic data consistent with *D. melanogaster*
438 populations. For a relatively short time since admixture, around 100 generations, it is
439 possible to obtain accurate and approximately unbiased estimates of the admixture time
440 over a wide range of ancestry proportions, indicating that this method may be applicable to

441 recently admixed human populations as well (Figure 9). Nonetheless, this result
442 underscores the need to examine biases associated with LD pruning in this approach prior
443 to application to a given dataset.
444
445 **Bias in LAI due to Uncertainty in Time of Admixture**
446 To demonstrate that assumptions about the number of generations since admixture have
447 the potential to bias LAI, we analyzed a SNP-array dataset from Greenlandic Inuits [51,52].
448 The authors had previously noted a significant impact of t on the LAI results produced
449 using RFMix [24], which we were able to reproduce here for chromosome 10 (Figure 10).
450 Indeed, even for comparisons between $t = 5$ and $t = 20$, both of which may be biologically
451 plausible for these populations, the mean difference in posterior probabilities between
452 samples estimated using RFMix was 0.0903 (Figure 10). However, when we applied our
453 method to these data, a clear optimum from t was obtained at approximately 6-7
454 generations prior to the present (Figure 10). This comparison therefore demonstrates that
455 even relatively minor changes in assumptions of t have the potential to strongly impact LAI
456 results, and underscores the importance of simultaneously performing LAI while
457 estimating t.
458
459 However, these results also indicate that our method may not be robust in situations where
460 the background LD is high and ancestry informative markers are neither common nor
461 distributed evenly across the genome. When we compared the results of our method a $t = 5$
462 and $t = 20$, we obtained similar differences in the mean posterior among individuals as with
463 RFMix. There are likely two causes. First, the datasets considered were generated with a

464 metabochip SNP-chip [53], which contains a highly non-uniform distribution of markers
465 across the genome. Second, the ancestral LD in the Inuit population is extensive [52], and
466 we could only retain a relatively small proportion of the markers after LD pruning in the
467 reference panels. These results therefore also underscore the challenges of LAI when the
468 signal to noise ratio is low.
469
470 **Patterns of LA on Inversion Bearing Chromosomes in *D. melanogaster***
471 Given their effects suppressing recombination in large genomic regions, chromosomal
472 inversions may be expected to strongly affect LAI [2,54]. Although we attempted to limit
473 the impact of chromosomal inversions by eliminating known polymorphic arrangements
474 from the reference panels (see methods), many known inversions are present within the
475 pool-seq samples we aimed to analyze [55]. We therefore focused on known inverted
476 haplotypes within the DGPR samples [54,56-58], which are comprised of inbred
477 individuals, and therefore phase is known across the entire chromosome.
478
479 In comparing LA estimates between inverted and standard arrangements, it is clear that
480 chromosomal inversions can substantially affect LA across the genomes (Figure 11). In
481 general, the chromosomal inversions considered in this work originated in African
482 populations of *D. melanogaster* [54], and consistent with this observation, most inversion
483 bearing chromosomes showed evidence for elevated African ancestry. This was
484 particularly evident in the regions surrounding breakpoints, where recombination with
485 standard arrangement chromosomes is most strongly suppressed. Importantly, this pattern
486 continued outside of inversion breakpoints as well, consistent with numerous observations

that recombination is repressed in heterokaryotypes in regions well outside of the inversion breakpoints in *Drosophila* (*e.g.* [2,54,59]). In(3R)Mo is an exception to this general pattern of elevated African ancestry within inverted arrangements (Figure 11). This inversion originated within a cosmopolitan population [54], and has only rarely been observed within sub-Saharan Africa [60,61]. Consistent with these observations, In(3R)Mo displayed lower overall African ancestry than chromosome arm 3R than standard arrangement chromosomes.

Although chromosomal inversions may affect patterns of LA in the genome on this ancestry cline, we believed including chromosomal inversions in the pool-seq datasets would not heavily bias our analysis of LA clines. Inversions tend to be low frequency in most populations studied [55], and because they affect LA in broad swaths of the genome—sometimes entire chromosome arms—including inversions is unlikely to affect LA cline outlier identification which appears to affect much finer scale LA (below). Furthermore, inversion breakpoint regions were not enriched for LA cline outliers in our analysis (Table 3), suggesting that inversions have a limited impact on overall patterns of local ancestry on this cline. Nonetheless, the LAI complications associated with chromosomal inversions should be considered when testing selective hypotheses for chromosomal inversions as genetic differentiation may be related to LA, rather than arrangement-specific selection in admixed populations such as those found in North America.

Table 3. LA clines in the genomic intervals immediately surrounding breakpoints of known polymorphic inversions.

Inversion	Breakpoint	Rho	p-value
	Distal	0.0298	0.923
In(2L)t	Proximal	-0.297	0.325
	Proximal	-0.0615	0.849
In(2R)NS	Distal	0.254	0.426
	Proximal	-0.336	0.261
In(3R)K	Distal	-0.686	0.00958
	Proximal	-0.494	0.0858
In(3R)Mo	Distal	-0.631	0.0207
	Proximal	0.193	0.527
In(3R)P	Distal	0.0789	0.798
	Distal	-0.0711	0.836
In(3L)P	Proximal	-0.222	0.511

Application to *D. melanogaster* Ancestry Clines

Finally, we applied our method to ancestry clines between cosmopolitan and African ancestry *D. melanogaster*. Genomic variation across two ancestry clines have been studied previously [21,34,36,47]. In particular, the cline on the east coast of North America has been sampled densely by sequencing large pools of individuals to estimate allele frequencies, and previous work has shown that the overall proportion of African ancestry is strongly correlated with latitude [21]. Consistent with this observation, we found a significant negative correlation for all chromosome arms between proportion of average African ancestry and latitude (rho = -0.891, -0.561, -0.912, -0.913, and -0.755, for 2L, 2R, 3L, 3R, and X respectively).

Although global ancestry proportions have previously been investigated in populations on this ancestry cline [21,34], these analyses neglected the potentially much richer information in patterns of LA across the genome. We therefore applied our method to these

526 samples. Because of the relatively recent dual colonization history of these populations and
527 subsequent mixing of genomes, a genome-wide ancestry cline is expected [21]. However,
528 loci that depart significantly in clinality from the genome-wide background levels may
529 indicate that natural selection is operating on a site linked to that locus.
530
531 **Clinality of LA is Strongly Correlated with Recombination Rate**
532 Previous studies have shown that regions of low recombination are disproportionately
533 resistant to admixture [7,17], a pattern that may reflect the fact that loci in low
534 recombination regions are more likely to be tightly linked in an admixed population to a
535 locus that is deleterious on admixed genetic backgrounds, or where one ancestry type is
536 disfavored in the local environment of the admixed population. Consistent with these
537 observations, we observed a significant positive correlation between the mean partial
538 correlation with latitude and local recombination rates across the genome (Table 4).
539 Furthermore, for only chromosome arm 3L did the 95% bootstrap confidence interval for
540 the correlation between LA clinality and recombination rate overlap with 0 (Table 4). All
541 other chromosome arms individually showed a significant positive correlation between LA
542 clinality and recombination rates, indicating that the correlation between LA clines and
543 local recombination rates in the genome is a robust relationship.
544
545 **Table 4.** Genome-wide and arm-specific correlation between recombination and the partial
546 correlation between LA proportion and latitude, including Spearman's Correlation, the p-
547 value for the observed correlation and the 95% bootstrap confidence interval.

Chromosome Arm	rho	p	2.5% Boostrap CI	97.5% Boostrap CI

All	0.1259436	0.0001167	0.084518662	0.20262254
2L	0.2434135	0.000691	0.08819046	0.346119464
2R	0.1839665	0.01633	0.032780198	0.3305687
3L	-0.0986359	0.1213	-0.207119717	0.059341699
3R	0.1649162	0.05151	0.000177156	0.323058668
X	0.2672564	0.0002651	0.166917018	0.445182509

548

549 One interpretation of this observation that clinality of LA is strongly correlated with local
550 recombination rates is that selection has had a substantial impact on the distribution of LA
551 in the *D. melanogaster* ancestry cline on the east coast of North America, and lends further
552 support to a growing consensus that low recombination regions may be especially unlikely
553 to introgress between ancestral populations presumably because negatively selected loci
554 have a greater effect on LA due to increased linkage between neutral and selected sites in
555 low recombination genomic regions.

556

557 **Outlier LA Clines**

558 Selection within admixed populations may take several distinct forms. On the one hand,
559 loci that are favorable in the admixed population—either because they are favored on an
560 admixed genetic background, enhance reproductive success in an admixed population, or
561 are favorable in the local environment—will tend to achieve higher frequencies, and we
562 would expect these sites to have a more positive correlation with latitude than the genome-
563 wide average. Conversely, loci that are disfavored within the admixed population may be
564 expected to skew towards a more negative correlation with latitude.

565

566 Although it is not possible to distinguish between these hypotheses directly, a majority of
567 evidence suggests that selection has primarily acted to remove African ancestry from the

largely Cosmopolitan genetic backgrounds found in this ancestry cline. First, abundant evidence suggests pre-mating isolation barriers between some African and cosmopolitan populations [62-64]. Second, there is strong post-mating isolation between populations on the ends of this cline [42,43]. Third, we report here a strong negative correlation between LA clines and local recombination rates (above). Finally, circumstantially, the local environment on the east coast of North America is perhaps most similar to Cosmopolitan than to African ancestral populations, which further suggests that Cosmopolitan alleles are likely favored through locally adaptive mechanisms. We therefore examined loci that are outliers for a negative partial correlation with latitude, as this is the expected pattern for African alleles that are disfavored in these populations.

There is an ongoing debate about the relative merits of an outlier approach versus more sophisticated models for detecting and quantifying selection in genome-wide scans. We believe that the difficulties of accurately estimating demographic parameters for this ancestry cline make the outlier approach most appealing for our purposes. Using our outlier approach, we identified 80 loci that showed the expected negative correlation with latitude (Figure 12). Although the specific statistical threshold that we employed is admittedly arbitrary, given the strength of evidence indicating widespread selection on ancestry in this species (above), we expected that the tail of the LA cline distribution would be enriched for the genetic targets of selection.

Differences Among Chromosome Arms

590 Due to the differences in inheritance, evolutionary theory predicts that selection will
591 operate differently on the X chromosome relative to autosomal loci. Of specific relevance to
592 this work, the large-X effect [65,66] is the observation that loci on the X chromosome
593 contribute to reproductive isolation at a disproportionately high rate. Additionally, and
594 potentially the cause of the large-X effect, due to the hemizygosity of X-linked loci, the X
595 chromosome is expected to play a larger role in adaptive evolution, the so-called faster-X
596 effect [67]. There is therefore reason to believe that the X chromosome will play a
597 significant role in genetically isolating Cosmopolitan and African *D. melanogaster*.
598
599 Consistent with a larger role for the sex chromosomes in generating reproductive isolation
600 or selective differentiation between *D. melanogaster* ancestral populations, we found that
601 that the X chromosome has a lower mean African ancestry proportion than the autosomes
602 in all populations. Furthermore, the X displayed a significantly higher rate of outlier LA loci
603 than the autosomes (23 LA outliers on the X, 57 on the Autosomes, $p = 0.0341$, one-tailed
604 exact Poisson test). Although consistent with evolutionary theory, differences between
605 autosomal arms and the X chromosome may also be explained in part by differences in per
606 base-pair recombination rates on the X chromosome than the autosomes, differences in
607 power to identify LA clines, or by the disproportionately larger number of chromosomal
608 inversions on the autosomes than on the X chromosome in these populations [55,60].
609
610 **Biological Properties of Outlier Loci**
611 We next applied gene ontology analysis to the set of outlier genes to identify common
612 biological attributes that may suggest more specific organismal phenotypes underlying LA

613 clinal outliers. We found modest enrichments in eight GO categories without the set of
614 clinal LA genes, however none remained significant after applying a multiple testing
615 correction (Table 5). Nonetheless, given the abundance of evidence supporting a role for
616 pre-mating isolation barriers between African and Cosmopolitan flies [62-64], the GO term,
617 behavior, is of interest. Consistent with this observation, one of the strongest LA cline
618 outliers, *egh*, has been conclusively linked to strong effects on male courtship behavior
619 using a variety of genetic techniques [68]. Additionally, gene knockouts of CG43759,
620 another LA cline outlier locus, have strong effects on inter-male aggressive behavior [69],
621 and may also contribute to behavioral differences between admixed individuals. These loci
622 are therefore appealing candidate genes for functional follow-up analyses, and illustrate
623 the power of this LAI approach for identifying candidate genes associated with differential
624 selection on ancestral variation in admixed populations.
625
626 **Table 5.** Signficant gene ontology terms for LA clinal outlier loci.

GO Term	Description	p-value	enrichment score
GO:0030054	cell junction	1.33E-04	7.6
GO:0005850	eukaryotic translation initiation factor 2 complex	2.10E-04	83.58
GO:0017177	glucosidase II complex	3.49E-04	66.86
GO:0007016	cytoskeletal anchoring at plasma membrane	8.86E-05	33.43
GO:0065008	regulation of biological quality	6.89E-04	2.63
GO:0007610	behavior	7.10E-04	3.36
GO:0051049	regulation of transport	9.38E-04	5.28
GO:0032507	maintenance of protein location in cell	9.84E-04	15.2

627

628 # Conclusion

A growing number of next-generation sequencing projects produce low coverage data that cannot be used to unambiguously assign individual genotypes, but which can be analyzed probabilistically to account for uncertainty in individual genotypes [70-72]. However, most existing LAI methods require genotype data derived from diploid individuals. Hence, there is an apparent disconnect between existing LAI approaches and the majority of ongoing sequencing efforts. In this work, we developed the first framework for applying LAI to pileup read data, rather than error-free genotypes, and we have generalized this model to arbitrary sample ploidies. This method therefore has immediate applications to a wide variety of existing and ongoing sequencing projects, and we expect that this approach and extensions thereof will be valuable to a number of researchers.

For many applications, a parameter of central biological interest is the time since admixture began (t). A wide variety of approaches have been developed that aim to estimate t and related parameters in admixed populations [26,28,29,73-76]. Many of these methods are based on an inferred distribution of tract lengths, however, inference of the ancestry tract length distribution is associated with uncertainty that is typically not incorporated in currently available methods for estimating t. Furthermore, incorrect assumptions regarding t has the potential to introduce biases during LAI. Hence, it is preferable to estimate demographic parameters such as the admixture time during the LAI procedure. Nonetheless, as noted above, although LAI using our method is robust to many deviations from the assumed model, admixture time estimates are sensitive to a variety of potential confounding factors and examining the resulting ancestry tract distributions after

LAI may be necessary to confirm that the assumed demographic model provides a reasonable fit to the data.

To our knowledge, this is the first method that attempts to simultaneously link LAI and population genetic parameter estimation directly, and we can envision many extensions of this approach that could expand the utility of this method to a broad variety of applications. For example, it is straightforward to accommodate additional reference populations (*e.g.* by assuming multinomial rather than binomial read sampling). Alternatively, any demographic or selective model that can be approximated as a Markov process could be incorporated—in particular, it is feasible to accommodate two-pulse admixture models and possibly models including ancestry tracts that are linked to positively selected sites. Such methods can be used to construct likelihood ratio tests of evolutionary models and for providing improved parameter estimates.

Methods

Constructing Emissions Probabilities

We model the ancestry using an HMM $\{H_v\}$ with state space $S = \{0,1,\ldots,n\}$, where $H_v = i$, $i \in S$, indicates that in the vth position i chromosomes are from population 0 and $n - i$ chromosomes are from population 1. In the following, to simplify the notation and without loss of generality, we will omit the indicator for the position in the genome as the structure of the model is the same for all positions of equivalent ploidy. We assume each variant site is biallelic, with two alleles A and a, and the availability of reference panels from source populations 0 and 1 with total allelic counts C_{0a}, C_{1a}, C_{0A}, and C_{1A}, where the two subscripts

refer to population identity and allele, respectively. Also, $C_0 = C_{0A} + C_{0a}$ and $C_1 = C_{1A} + C_{1a}$. Finally, we also assume we observe a pileup of r reads from the focal population, with r_A and r_a reads for alleles A and a respectively ($r = r_A + r_a$). The emission probability of state $i \in S$ of the process is then defined as $e_i = \Pr(r_A, C_{0A}, C_{1A} \mid r, C_0, C_1, H = i, \varepsilon)$, where ε is an error rate. This probability can be calculated by summing over all possible genotypes in the admixed sample and over all possible population identities of the reads, as explained in the following section.

The probability of obtaining r_0 ($=r - r_1$) reads, in the admixed population, from chromosomes of ancestry 0, given r and the hidden state $H = i$, and assuming no mapping or sequencing biases, is binomial,

$$r_0 \mid H = i, n, r \sim \mathrm{Bin}(r, i/n)$$

These probabilities are pre-computed in our implementation for all possible values of $i \in S$ and $r_0, 0 \le r_0 \le r$. Similarly, for the reference populations, for j=0,1,

$$C_{jA} \mid C_j, f_j \sim \mathrm{Bin}(C_j, f_j)$$

where f_j is the allele frequency of allele A in population j. The analogous allelic counts in the admixed population, denoted C_{M0a}, C_{M1a}, C_{M0A}, and C_{M1A}, are unobserved (only reads are observed for the admixed population), but are also conditionally binomially distributed, *i.e.*:

697 $$C_{M0A} \mid H = i, f_0 \sim \mathrm{Bin}(i, f_0) \text{ and } C_{M1A} \mid H = i, n, f_1 \sim \mathrm{Bin}(n - i, f_1)$$

698

699 Finally, in the absence of errors, and assuming no sequencing or mapping biases, the

700 conditional probability of obtaining r_{0A} reads of allele A in the admixed population is

701

702 $$r_{0A} \mid H = i, r_0, C_{M0A} \sim \mathrm{Bin}(r_0, C_{M0A} / i)$$

703

704 This probability can be expanded to include errors, in particular assuming a constant and

705 symmetric error rate ε between major and minor allele, and assuming all reads with

706 nucleotides that are not defined as major or minor are discarded, we have

707

708 $$r_{0A} | H = i, r_o, C_{M0A}, \varepsilon \sim \mathrm{Bin}(r_0, (1-\varepsilon)C_{M0A}/i + \varepsilon(1 - C_{M0A}/i)).$$

709

710 Using these expressions, and integrating over allele frequencies in the source populations,

711 we have

$$\Pr(r_{0A}, C_{0A,} | r_0, C_0, n, H = i, \varepsilon) =$$

712 $$\int_0^1 \sum_{k=0}^{i} \Pr(r_{0A} | H = i, r_0, C_{M0A} = k, \varepsilon) \Pr(C_{M0A} = k | H = i, f_0) p(f_0) df_0 \quad =$$

713

$$\frac{C_0!\, i!}{(C_0 - C_{0A})!\, C_{0A}!\, (C_0 + i + 1)!} \sum_{k=0}^{i} \Pr(r_{0A} | H = i, r_0, C_{M0A}$$

$$= k, \varepsilon) \frac{(C_0 - C_{0A} + i - k)!\, (C_{0A} + k)!}{(i - k)!\, k!}$$

714

715

716 assuming a uniform [0, 1] distribution for f_0. A similar expression is obtained for

717 $\Pr(r_{1A}, C_{1A,}|r_1, C_1, n, H = i, \varepsilon)$, assuming $f_1 \sim \mathrm{U}[0,1]$, and these expressions combine

718 multiplicatively to give

719

$$\Pr(r_A, C_{1A,}, C_{0A,}|r_0, C_0, r_1, C_1, n, H = i, \varepsilon) =$$

720 $$\sum_{r_{0A}=\max\{0, r_A - r_1\}}^{\min\{r_0, r_A\}} \Pr(r_{0A}, C_{0A,}|r_0, C_0, n, H = i, \varepsilon) \Pr(r_{1A} = r_A - r_{0A}, C_{1A,}|r_1, C_1, n, H = i, \varepsilon),$$

721

722 and the emission probabilities become

723

724 $\Pr(r_A, C_{0A}, C_{1A} \mid r, C_0, C_1, H = i, \varepsilon) =$

$$\sum_{r_0=0}^{r} \Pr(r_0|H = i, n, r) \Pr(r_A, C_{1A,}, C_{0A,}|r_0, C_0, r_1 = r - r_0, C_1, n, H = i, \varepsilon)$$

725

726 Alternatively, if the sample genotypes are known with high confidence, i.e. $C_{MA} = C_{M0A} + C_{M1A}$

727 is observed, the emission probabilities are the defined as

728

729 $$\Pr(C_{MA}, C_{0A}, C_{1A} \mid C_0, C_1, n, H = i) =$$
$$\binom{C_0}{C_{0A}}\binom{C_1}{C_{1A}} \sum_{k=\max\{C_{MA}-i,0\}}^{\min\{n-i, C_{MA}\}} \int_0^1 \binom{n-i}{k} (f_0)^{C_{0A}+k} (1-f_0)^{C_0+n-i-C_{0A}-k} df_0 \int_0^1 \binom{i}{C_{MA}-k} (f_1)^{C_{MA}-k+C_{1A}} (1-f_1)^{C_1+i-C_{1A}-C_{MA}+k} df_1$$
$$= \sum_{k=\max\{C_{MA}-i,0\}}^{\min\{n-i, C_{MA}\}} \frac{C_0!C_1!i!(n-i)!(C_{MA}+C_{1A}-k)!(C_{0A}+k)!(C_1-C_{MA}-C_{1A}+i+k)!(C_0-C_{0A}-i-k+n)!}{(C_0-C_{0A})!C_{0A}!(C_1-C_{1A})!C_{1A}!(C_{MA}-k)!k!(k+i-C_{MA})!(n-k-i)!(n-i+C_0+1)!(i+C_1+1)!}$$

730

These emissions probabilities are sometimes substantially faster to compute than those for short read pileups, especially when sequencing depths are high. However, the genotypes must be estimated with high accuracy for this approach to be valid. For applications with low read coverage, or with ploidy >2 for which many standard genotype callers are not applicable, it is usually preferable to use the pileup-based approach described above.

Constructing Transition Probabilities

We assume an admixed population, of constant size, with N diploid individuals, in which a proportion m of the individuals in the population where replaced with migrants t generations before the time of sampling. Given these assumptions, and an SMC' model of the ancestral recombination graph [77], the rate of transition from ancestry 0 to 1, along the length of a single chromosome, is

$$\lambda_0 = 2Nm\left(1 - e^{\frac{-t}{2N}}\right)$$

per Morgan [50]. Similarly, the rate of transition from ancestry 1 to 0 on a single chromosome is

$$\lambda_1 = 2N\left(1-m\right)\left(1 - e^{\frac{-t}{2N}}\right)$$

751 per Morgan. Importantly, because these expressions are based on a coalescence model,
752 they account for the possibility that a recombination event occurs between two tracts of
753 the same ancestry type and the probability that the novel marginal genealogy will back-
754 coalesce with the previous genealogy [50]. Both events are expected to decrease the
755 number of ancestry switches along a chromosome and ignoring their contribution will
756 cause overestimation of the rate of change between ancestry types between adjacent
757 markers.
758
759 The transition rates are in units per Morgan, but can be converted to rates per bp, by
760 multiplying with the recombination rate in Morgans/bp, r_{bp} within a segment. The
761 transition probabilities of the HMM for a single chromosome, $\mathbf{P}(l) = \{P_{ij}(l)\}, i, j \in S$, between
762 two markers with a distance l between each other, is then approximately
763

764
$$\mathbf{P}(l) = \begin{bmatrix} 1-\lambda_0 r_{bp} & \lambda_0 r_{bp} \\ \lambda_1 r_{bp} & 1-\lambda_1 r_{bp} \end{bmatrix}^l$$

765
766 using discrete distances, or
767
768

769
$$\mathbf{P}(l) = \begin{bmatrix} \frac{\lambda_1}{\lambda_0+\lambda_1} + \frac{\lambda_0}{\lambda_0+\lambda_1} e^{-r_{bp} l (\lambda_0+\lambda_1)} & \frac{\lambda_0}{\lambda_0+\lambda_1} - \frac{\lambda_0}{\lambda_0+\lambda_1} e^{-r_{bp} l (\lambda_0+\lambda_1)} \\ \frac{\lambda_0}{\lambda_0+\lambda_1} + \frac{\lambda_1}{\lambda_0+\lambda_1} e^{-r_{bp} l (\lambda_0+\lambda_1)} & \frac{\lambda_1}{\lambda_0+\lambda_1} - \frac{\lambda_1}{\lambda_0+\lambda_1} e^{-r_{bp} l (\lambda_0+\lambda_1)} \end{bmatrix}$$

using continuous distances along the chromosome. Here, we use the continuous representation for calculations. We emphasize that the assumption of a Markovian process is known to be incorrect [50], in fact admixture tracts tend to be more spatially correlated than predicted by a Markov model, and the degree and structure of the correlation depends on the demographic model [50]. Deviations from a Markovian process may cause biases in the estimation of parameters such as *t*.

The Markov process defined above is applicable to a single chromosome. We now want to approximate a similar process for a sample of *n* chromosomes from a single sequencing pool. The true process is quite complicated, and we choose for simplicity to approximate the process for *n* chromosomes sampled from one population, as the union of *n* independent chromosomal processes. We will later quantify biases arising due to this independence assumption using simulations. Under the independence assumption, the transition probability from *i* to *j* is simply the probability of *l* transitions from state 1 to state 0 in the marginal processes and $j - i + l$ transitions from state 0 to state 1, summed over all admissible values of *l*, i.e.,

$$\Pr\left(H_{v+k} = j \mid H_v = i\right) = \sum_{l=\max\{0,i-j\}}^{\min\{n-j,i\}} \binom{n-i}{j-i+l} \left(P_{01}(k)\right)^{j-i+l} \left(1-P_{01}(k)\right)^{n-j+i-l} \binom{i}{l} \left(P_{10}(k)\right)^{l} \left(1-P_{10}(k)\right)^{i-l}$$

790 Although this procedure can be computationally expensive when there are many markers,
791 read depths are high, and especially when n is large, in our implementation, we reduce the
792 compute time by pre-calculating and storing all binomial coefficients.
793
794 **Estimating Time Since Admixture**
795 A parameter of central biological interest, that is often unknown in practice, is the time
796 since the initial admixture event (t). We therefore use the HMM representation to provide
797 maximum likelihood estimates of t using the forward algorithm to calculate the likelihood
798 function. As this is a single parameter optimization problem for a likelihood function with a
799 single mode, optimization can be performed using a simple golden section search [78].
800 Default settings for this optimization in our software, including the search range maxima
801 defaults, t_{max} and $t_{min,}$ are documented in the C++ HMM source code provided at
802 https://github.com/russcd/Ancestry_HMM.
803
804 **Posterior Decoding**
805 After either estimating or providing a fixed value of the time since admixture to the HMM,
806 we obtained the posterior distribution for all variable sites considered in our analysis using
807 the forward-backward algorithm, and we report the full posterior distribution for each
808 marker along the chromosome.
809
810 **Simulating Ancestral Polymorphism**
811 To validate our HMM, we generated sequence data for each of two ancestral populations
812 using the coalescent simulator MACS [79]. We sought to generate data that could be

consistent with that observed in Cosmopolitan and African populations of *D. melanogaster*, which has been studied previously in a wide variety of contexts [2,11,31-33]. We used the command line "macs 400 10000000 -i 1 -h 1000 -t 0.0376 -r 0.171 -c 5 86.5 -I 2 200 200 0 -en 0 2 0.183 -en 0.0037281 2 0.000377 -en 0.00381 2 1 -ej 0.00382 2 1 -eN 0.0145 0.2" to generate genotype data. This will produce 200 samples of ancestry 0 and 200 samples of ancestry 1 on a 10mb chromosome—*i.e.* this should resemble genotype data for about half of an autosomal chromosome arm in *D. melanogaster*. Unless otherwise stated below, we then sampled the first 50 chromosomes from each ancestral population as the ancestral population reference panel, whose genotypes are assumed to be known with low error rates. The sample size was chosen because it is close to the size of the reference panel that we obtained in our application of this approach to *D. melanogaster* (below).

To evaluate the performance of our method on data consistent with human populations, we simulated data that could be consistent with that observed for modern European and African human populations. Specifically, we simulated the model of [80] using the command line "macs 200 1e8 -I 3 100 100 0 -n 1 1.682020 -n 2 3.736830 -n 3 7.292050 -eg 0 2 116.010723 -eg 1e-12 3 160.246047 -ma x 0.881098 0.561966 0.881098 x 2.797460 0.561966 2.797460 x -ej 0.028985 3 2 -en 0.028986 2 0.287184 -ema 0.028987 3 x 7.293140 x 7.293140 x x x x x -ej 0.197963 2 1 -en 0.303501 1 1 -t 0.00069372 -r 0.00069372". Admixture between ancestral populations was then simulated as described below.

Simulating Admixed Populations

836 Although it is commonly assumed that admixture tract lengths can be modeled as
837 independent and identically distributed exponential random variables (e.g. [26,29] and in
838 this work, above), this assumption is known to be incorrect as ancestry tracts are neither
839 exponentially distributed, independent across individuals, nor identically distributed along
840 chromosomes [50]. We therefore aim to determine what bias violations of this assumption
841 will have on inferences obtained from this model. Towards this, we used SELAM [81] to
842 simulate admixed populations under the biological model described above. Because this
843 program simulated admixture in forward time, it generates the full pedigree-based
844 ancestral recombination graph, and is therefore a conservative test of our approach
845 relative to the coalescent which is known to produce incorrect ancestry tract distributions
846 for short times [50]. Briefly, we initialized each admixed population simulation with a
847 proportion, *m*, of ancestry from ancestral population 1, and a proportion 1-*m* ancestry from
848 ancestral population 0. Unless otherwise stated, all simulations were conducted with
849 neutral admixture and a hermaphroditic diploid population of size 10,000.
850
851 We then assigned the additional, non-reference chromosomes from the coalescent
852 simulations, to each ancestry tract produced in SELAM simulations according to their local
853 ancestry along the chromosome. In this way, each chromosome is a mosaic of the two
854 ancestral subpopulations. See, *e.g.* [2], for a related approach for simulating genotype data
855 of admixed chromosomes.
856
857 **Pruning Ancestral Linkage Disequilibrium**

858 Correlations induced by LD between markers within ancestral populations violates a
859 central assumption of the Markov model framework. Although it may be feasible to
860 explicitly model linkage within ancestral populations, when ancestral populations have
861 relatively little LD, such as those of *D. melanogaster*, another effective approach is to
862 discard sites that are in strong LD in the ancestral populations. Hence, to avoid this
863 potential confounding aspect of the data, we first computed LD between all pairs of
864 markers within each reference panel that are within 0.01 centimorgans of one another. We
865 then discarded one of each pair of sites where $|r|$ in either reference panel exceeded a
866 particular threshold, and we decreased this threshold until we obtained an approximately
867 unbiased estimate of the time since admixture estimates of the HMM. This approach differs
868 from a previous method, LAMPanc, where LD is pruned from within admixed samples (see
869 also below).
870
871 **Simulating Sequence Data**
872 We first identified all sites where the allele frequencies of the ancestral populations differ
873 by at least 20% within the reference panels. We excluded weakly differentiated sites to
874 decrease runtime and because these markers carry relatively little information about the
875 LA at a given site. Then, to generate data similar to what would be produced using Illumina
876 sequencing platforms, we simulated allele counts for each sample, by first drawing the
877 depth at a given site from a Poisson distribution. In most cases and unless otherwise stated,
878 the mean of this distribution is set to be equal to the sample ploidy. We did this to ensure
879 equivalent sequencing depth per chromosome regardless of pooling strategy, and because
880 this depth is sufficiently low that high quality genotypes cannot be determined. We then

generated set of simulated aligned bases via binomial sampling from the sample allele frequency and included a uniform error rate of 0.5% for both alleles at each site.

Unless otherwise stated, we simulated a total of 40 admixed chromosomes. The HMM can perform LAI on more than one sample at a time, and we therefore included all samples when running it. Hence, we used 40 haploid, 20 diploid, 4 pools of 10 chromosomes, and 2 pools of 20 chromosomes for most comparisons of accuracy reported below, unless otherwise stated.

Accuracy Statistics

To evaluate the performance of the HMM, we computed four statistics. First, we compute the proportion of sites where the true state is within the 95% posterior credible interval, where ideally, this proportion would be equal to or greater than 0.95. Second, we compute the mean posterior error, the average distance between the posterior distribution of hidden states and the true state

$$E = \frac{\sum_{v=0}^{S}\sum_{i=0}^{n} p\left(H_v = i \mid \mathbf{r}\right)\left|i - I_v\right|}{k}$$

Here S is the total number of sites, I_v is the true state at site v, and $\mathbf{r}$ is all the combined read data. Third, we also report the proportion of sites where the maximum likelihood estimate of the hidden state is equal to the true ancestry state. Finally, as an indicator of the specificity of our approach, we also report the average width of the 95% credible interval.

903

904 **Deviations from the Assumed Neutral Demographic Model**

905 A potential issue with this framework is that the assumptions underlying the transition
906 matrixes and related time of admixture estimation procedure is likely to be violated in a
907 number of biologically relevant circumstances. We therefore simulated populations
908 wherein individuals of ancestral population 1 began entering a population entirely
909 composed of individuals from ancestral population 0, at a time *t* generations before the
910 present, at a constant rate that is sustained across all subsequent generations until the time
911 of sampling. That is, additional unadmixed individuals of ancestry 1 migrate each
912 generation from *t* until the present.

913

914 Natural selection acting on admixed genetic regions has been inferred in a wide variety of
915 systems (*e.g.* [5,7,13,17,18]), and is expected to have pronounced effects on the distribution
916 of LA among individuals within admixed populations. Here again, this aspect of biologically
917 realistic populations will tend to violate central underlying assumptions of the model
918 assumed in this work. Towards this, we simulated admixed populations with a single pulse
919 of admixture *t* generations prior to the time of sampling. We then incorporated selection at
920 2,5,10, and 20 loci at locations uniformly distributed along the length of the chromosome
921 arm. All selected loci were assumed to be fixed within each ancestral population. Selection
922 was additive and selective coefficients were assigned based on a uniform [0.005, 0.05]
923 distribution to either ancestry 0 or 1 alleles with equal probability. As above, these
924 simulations were conducted using SELAM [81].

925

For both selected and continuous migration simulations, we then performed the genotype and read data simulation procedure, and reran our HMM as described above. We performed 10 simulations for each treatment.

Comparisons to LAMPanc

We next sought to compare our method to a commonly used local ancestry inference method, LAMPanc [23]. Towards this, we again simulated data using MACS and SELAM as described above. For these comparisons, the initial ancestry contribution was 0.5 and the number of generations since admixture varied between 5 and 1000. For comparison, we supplied LAMPanc and our program the correct time since admixture and ancestry proportions, as these are required parameters for LAMPanc. We also supplied the program error free genotypes, another requirement of LAMPanc, whereas we supplied our HMM with read data simulated as described above. We then ran LAMPanc under default parameters, and we also reran LAMPanc using LD pruning within the reference panels, as we do in our method, instead of the default LD pruning implemented in LAMPanc.

Analysis of Inuit Genotype Data

To demonstrate that LAI methods can be biased by the arbitrary selection of the time since admixture, we analyzed a dataset of SNP-array genotype data from Greenlandic Inuits. These data are described in detail elsewhere [51,52]. This population has received some admixture from a European source population, and the authors had previously used RFMix [24] to perform LAI, and found some sensitivity to the assumed time since admixture (J. Crawford *pers. Comm.*). We analyzed data from chromosome 10 using RFMix v1.5.4 [24] as

949 described in Moltke *et al.* [52] assuming admixture occurred either 5 or 20 generations ago.
950 We subsequently analyzed chromosome 10 using our HMM including the genotype-
951 analysis emissions probabilities and assuming a genotype error rate of 0.2%. For our
952 analysis we identified the LD cutoff that is appropriate for these data as described above.
953
954 **Generating *D. melanogaster* Reference Populations**
955 To generate reference panels, we used a subset of the high quality *D. melenaogaster*
956 assemblies that have been described previously in Pool *et al.* (2012) and Lack *et al.* (2015).
957 As in the local ancestry analysis of Pool (2015), we used the French population. For our
958 African reference panel, we selected a subset of the Eastern and Western African
959 populations (CO, RG, RC, NG, UG, GA, GU) and grouped them into a single population for the
960 purposes of our analysis. We elected to combine populations so that we would have a
961 larger reference panel of African populations for this analysis, this solution may be justified
962 because these *D. melanogaster* populations are only weakly genetically differentiated
963 [2,21,82], particularly after common inversion-bearing chromosomes are removed from
964 analyses. Specific individuals were selected for inclusion in the African reference panel if
965 previous work found they have relatively little cosmopolitan ancestry (*i.e.* below 0.2
966 genome-wide in [2]).
967
968 Because of their powerful effects on recombination, chromosomal inversions are known to
969 have substantial impacts on the distribution of genetic variants on chromosomes
970 containing chromosomal inversions in *D. melanogaster* [2,54]. For this reason, we removed
971 all common inversion-bearing chromosome arms from the reference populations [83].

Nonetheless, it is clear that chromosomal inversions are present in the pool-seq samples [55]. Although the inversions certainly violate key assumptions of our model—particularly the transmission probabilities—given that our approach is robust to a many perturbations, we expect the LA within inverted haplotypes can be estimated with reasonable confidence, and the overall LAI procedure will still perform adequately with low frequencies of chromosomal-inversion bearing chromosomes present within these samples.

Although these reference populations are believed to have relatively little admixture, some admixture is likely to remain within these samples [2]. To mitigate this potential issue, we first applied our HMM to each reference population using the genotype-based emissions probabilities (above). Calculated across all individuals, we found that our maximum likelihood ancestry estimates were identical with those of Pool *et al.* (2012) at 96.2% of markers considered in our analysis. The differences between the results of these methods may reflect differences in the methodology of LAI or differences in the reference panels. Nonetheless, the broad concordance suggests the two methods are yielding similar overall results. We masked all sites where the posterior probability of non-native ancestry was greater than 0.5 within each reference individual's genome. These masked sequences were then used as the reference panel for the analyses of poolseq data below.

Ancestry Cline Sequence Data Analysis

We acquired pooled sequencing data from six populations from the east coast of the United States. The generation of these samples, sequencing data, and accession numbers are described in detail in [21,36]. Briefly, the samples are comprised of individuals drawn from

natural populations and sequenced in relatively large pools of 66-232 chromosomes. We aligned all data using BWA v0.7.9a-r786 [84] using the 'MEM' function and the default program parameters. For all alignments, we used version 5 of the *D. melanogaster* reference genome [85] in order to make our analysis and coordinates compatible with the *Drosophila* genome nexus [83]. We then realigned all reads using the indelrealigner tool within the GATK package [72], and we extracted the sequence pileup using samtools mpileup v1.1 [86] using the program's default parameters.

We extracted sites at ancestry informative positions within the reference panels, where we required that the reference panel have a minimum of 50% of individuals with a high quality genotype call in both Cosmopolitan and African reference populations. As above, ancestry informative sites were defined as those with a minimum of 20% difference in allele frequencies between the reference panels used, and we retained only ancestry informative sites for our analyses. We then produced global ancestry estimates for each chromosome arm separately for each sample using the method of Bergland *et al.* (2016). We ran our HMM for each chromosome arm and each population, and we provided the program this estimate of the ancestry proportion and the time since admixture, 1593 generations [17]. We elected to provide the time since admixture because we have found that this parameter is difficult to estimate in relatively large pools (see Results). However, the program can accurately estimate LA in high ploidy samples even when the time since admixture cannot be estimated correctly (see Results).

Correlation with Local Recombination Rates

To assess the correlation between local recombination rates and clinality of LA clines in the genome, we employed a regression approach. First, we computed the mean partial correlation between latitude and local ancestry in windows of 100 ancestry informative markers. We then annotated the recombination rate in the midpoint of that genomic window, where as above, we used the recombination rate estimates of [87]. We computed Spearman's correlation between local recombination rates and the mean partial correlation between LA and latitude for the whole genome and for each chromosome arm independently. We also estimated confidence intervals using 1000 block-bootstrap samples using window sizes of 100 SNPs.

Identifying LA Cline Outliers

To detect loci that show evidence for steeper ancestry clines than the genomic average, we first computed the Spearman's rank correlation between mean ancestry proportions and latitude for each chromosome arm separately. Then, for each site for which we obtained a posterior ancestry distribution for all samples, we computed the partial Spearman's rank correlation between the posterior ancestry mean and latitude while correcting for the correlation between latitude and the overall ancestry proportion. We then computed the probability of obtaining the observed partial correlation in R, which implements the approach of [88], and we retained those sites where the probability of the partial correlation between local ancestry and latitude was less than 0.005 as significant in our analysis. Although this cutoff is arbitrary, given the strong evidence for local adaptation and reproductive isolation in these populations [42,43,89], the tail of the LA cline distribution will likely be enriched for sites experiencing selection on this ancestry

gradient. Due to linkage, adjacent sites show strong autocorrelation. We therefore selected the local optima for a given clinally significant LA segment (*i.e.* a tract where all positions are significantly correlated with latitude at our threshold) and retained these for analyses of outlier loci. Finally, to further reduce the effect of autocorrelation, we retained only those local optima for which no other optimum had a stronger correlation with latitude within 100,000bp on either side on the site.

Gene Ontology Analyses

We performed Gene-ontology (GO) analyses of the set of clinal outlier loci where the background set was all genes located on any euchromatic chromosome arms in the *D. melanogaster* genome. The foreground set was defined as the gene intersected by a LA outlier local optimum, or the nearest gene to a local optimum. All GO analyses were performed using GOrilla [90].

Acknowledgements

We thank Tyler Linderoth, Shelbi Russell and members of the Nielsen and Slatkin labs for helpful comments. We also thank Jacob Crawford for providing Inuit polymorphism data and for providing the observation that LAI inference depended heavily on *t.*

References

1. Kronforst MR, Young LG, Blume LM, Gilbert LE. Multilocus analyses of admixture and introgression among hybridizing *Heliconius* butterflies. Evolution. 2006;60: 1254–16. doi:10.1554/06-005.1

2. Pool JE, Corbett-Detig RB, Sugino RP, Stevens KA, Cardeno CM, Crepeau MW, et al. Population genomics of sub-Saharan Drosophila melanogaster: African diversity and non-African admixture. PLoS Genet. 2012;8: e1003080–24. doi:10.1371/journal.pgen.1003080

3. Hufford MB, Lubinksy P, Pyhäjärvi T, Devengenzo MT, Ellstrand NC, Ross-Ibarra J. The genomic signature of crop-wild introgression in maize. PLoS Genet. 2013;9: e1003477–13. doi:10.1371/journal.pgen.1003477

4. Brandvain Y, Kenney AM, Flagel L, Coop G, Sweigart AL. Speciation and introgression between Mimulus nasutus and Mimulus guttatus. PLoS Genet. 2014;10: e1004410–15. doi:10.1371/journal.pgen.1004410

5. Rieseberg LH, Raymond O, Rosenthal DM, Lai Z, Livingstone K, Nakazato T, et al. Major ecological transitions in wild sunflowers facilitated by hybridization. Science. 2003;301: 1211–1216. doi:10.1126/science.1086949

6. Green RE, Krause J, Briggs AW, Maricic T, Stenzel U, Kircher M, et al. A draft sequence of the neandertal genome. Science. 2010;328: 710–722. doi:10.1126/science.1188021

7. Sankararaman S, Mallick S, Dannemann M, Prüfer K, Kelso J, Pääbo S, et al. The genomic landscape of Neanderthal ancestry in present-day humans. Nature. 2014;507: 354–357. doi:10.1038/nature12961

8. Price AL, Patterson NJ, Plenge RM, Weinblatt ME, Shadick NA, Reich D. Principal

components analysis corrects for stratification in genome-wide association studies. Nat Genet. 2006;38: 904–909. doi:10.1038/ng1847

9. Lohmueller KE, Pearce CL, Pike M, Lander ES, Hirschhorn JN. Meta-analysis of genetic association studies supports a contribution of common variants to susceptibility to common disease. Nat Genet. 2003;33: 177–182. doi:10.1038/ng1071

10. Freedman ML, Reich D, Penney KL, McDonald GJ, Mignault AA, Patterson N, et al. Assessing the impact of population stratification on genetic association studies. Nat Genet. 2004;36: 388–393. doi:10.1038/ng1333

11. Caracristi G, Schlotterer C. Genetic differentiation between American and European Drosophila melanogaster populations could be attributed to admixture of African alleles. Mol Biol Evol. 2003;20: 792–799. doi:10.1093/molbev/msg091

12. Kolbe JJ, Glor RE, Schettino LR, Lara AC, Larson A. Genetic variation increases during biological invasion by a Cuban lizard. Nature. 2004;431: 177–181.

13. Consortium THG, Consortium G. Butterfly genome reveals promiscuous exchange of mimicry adaptations among species. Nature. 2012;487: 94–98. doi:10.1038/nature11041

14. Racimo F, Sankararaman S, Nielsen R, Huerta-Sanchez E. Evidence for archaic adaptive introgression in humans. Nat Rev Genet. 2015;16: 359–371. doi:10.1038/nrg3936

15. Juric I, Aeschbacher S, Coop G. The strength of selection against Neanderthal

1104 introgression. bioRxiv. 2015 Oct pp. 1–24. doi:10.1101/030148

1105 16. Harris K, Nielsen R. The genetic cost of neanderthal introgression. Genetics. Genetics;
1106 2016;203: 881–891. doi:10.1534/genetics.116.186890

1107 17. Pool JE. The mosaic ancestry of the Drosophila Genetic Reference Panel and the D.
1108 melanogaster reference genome reveals a network of epistatic fitness interactions.
1109 Mol Biol Evol. 2015; msv194–16. doi:10.1093/molbev/msv194

1110 18. Schumer M, Cui R, Powell DL, Dresner R, Rosenthal GG, Andolfatto P. High-resolution
1111 mapping reveals hundreds of genetic incompatibilities in hybridizing fish species.
1112 eLife. 2014;3: 610–21. doi:10.7554/eLife.02535

1113 19. Pritchard JK, Stephens M, Donnelly P. Inference of population structure using
1114 multilocus genotype data. Genetics. 2000;155: 945–959.

1115 20. Skotte L, Korneliussen TS, Albrechtsen A. Estimating individual admixture
1116 proportions from next generation sequencing data. Genetics. 2013;195: 693–702.
1117 doi:10.1534/genetics.113.154138/-/DC1

1118 21. Bergland AO, Tobler R, González J, Schmidt P, Petrov D. Secondary contact and local
1119 adaptation contribute to genome-wide patterns of clinal variation in Drosophila
1120 melanogaster. Mol Ecol. 2016;25: 1157–1174. doi:10.1111/mec.13455

1121 22. Falush D, Stephens M, Pritchard JK. Inference of population structure using
1122 multilocus genotype data: linked loci and correlated allele frequencies. Genetics.
1123 2003;164: 1567–1587.

1124 23. Sankararaman S, Sridhar S, Kimmel G, Halperin E. Estimating local ancestry in
1125 admixed populations. Am J Hum Genet. 2008;82: 290–303.
1126 doi:10.1016/j.ajhg.2007.09.022

1127 24. Maples BK, Gravel S, Kenny EE, Bustamante CD. RFMix: a discriminative modeling
1128 approach for rapid and robust local-ancestry inference. Am J Hum Genet. 2013;93:
1129 278–288. doi:10.1016/j.ajhg.2013.06.020

1130 25. Baran Y, Pasaniuc B, Sankararaman S, Torgerson DG, Gignoux C, Eng C, et al. Fast and
1131 accurate inference of local ancestry in Latino populations. Bioinformatics. 2012;28:
1132 1359–1367. doi:10.1093/bioinformatics/bts144

1133 26. Pool JE, Nielsen R. Inference of historical changes in migration rate from the lengths
1134 of migrant tracts. Genetics. 2009;181: 711–719. doi:10.1534/genetics.108.098095

1135 27. Koopman W, Li Y, Coart E. Linked vs. unlinked markers: multilocus microsatellite
1136 haplotype-sharing as a tool to estimate gene flow and introgression. Mol Ecol.
1137 2007;16: 243–256. doi:10.1111/j.1365-294X.2006.03137.x

1138 28. Patterson N, Hattangadi N, Lane B. Methods for high-density admixture mapping of
1139 disease genes. Am J Hum Genet. 2004;74: 979–1000.

1140 29. Gravel S. Population Genetics Models of Local Ancestry. Genetics. 2012;191: 607–
1141 619. doi:10.1534/genetics.112.139808

1142 30. Consortium 1GP, BGI-Shenzhen, European Bioinformatics Institute, Illumina,
1143 Hospital BAW, College B, et al. An integrated map of genetic variation from 1,092

human genomes. Nature. 2012. doi:10.1038/nature11632

31. Haddrill PR, Thornton KR, Charlesworth B, Andolfatto P. Multilocus patterns of nucleotide variability and the demographic and selection history of Drosophila melanogaster populations. Genome Res. 2005;15: 790–799. doi:10.1101/gr.3541005

32. Thornton K, Andolfatto P. Approximate Bayesian inference reveals evidence for a recent, severe bottleneck in a Netherlands population of Drosophila melanogaster. Genetics. 2006;172: 1607–1619. doi:10.1534/genetics.105.048223

33. Li H, Stephan W. Inferring the demographic history and rate of adaptive substitution in Drosophila. PLoS Genet. 2006;2: e166. doi:10.1371/journal.pgen

34. Duchen P, Živković D, Hutter S, Stephan W. Demographic inference reveals African and European admixture in the North American Drosophila melanogaster population. Genetics. 2013;193: 291–301. doi:10.1534/genetics.112.145912/-/DC1

35. Langley CH, Stevens K, Cardeno C, Lee YCG, Schrider DR, Pool JE, et al. Genomic variation in natural populations of Drosophila melanogaster. Genetics. 2012;192: 533–598. doi:10.1534/genetics.112.142018

36. Bergland AO, Behrman EL, O'Brien KR, Schmidt PS, Petrov DA. Genomic evidence of rapid and stable adaptive oscillations over seasonal time scales in Drosophila. PLoS Genet. 2014;10: e1004775–19. doi:10.1371/journal.pgen.1004775

37. Schrider DR, Hahn MW, Begun DJ. Parallel evolution of copy-number variation across continents in Drosophila melanogaster. Mol Biol Evol. 2016;33: 1308–1316.

1164 doi:10.1093/molbev/msw014

1165 38. Reinhardt JA, Kolaczkowski B, Jones CD, Begun DJ, Kern AD. Parallel geographic
1166 variation in Drosophila melanogaster. Genetics. 2014;197: 361–373.
1167 doi:10.1534/genetics.114.161463/-/DC1

1168 39. Fabian DK, Kapun M, Nolte V, Kofler R, Schmidt PS, Schlotterer C, et al. Genome-wide
1169 patterns of latitudinal differentiation among populations of Drosophila
1170 melanogasterfrom North America. Mol Ecol. 2012;21: 4748–4769.
1171 doi:10.1111/j.1365-294X.2012.05731.x

1172 40. Oakeshott JG, Gibson JB, Anderson PR, Knibb WR. Alcohol dehydrogenase and
1173 glycerol-3-phosphate dehydrogenase clines in Drosophila melanogaster on different
1174 continents. Evolution. 1982;36: 86–96.

1175 41. Berry A, Kreitman M. Molecular analysis of an allozyme cline: alcohol dehydrogenase
1176 in Drosophila melanogaster on the east coast of North America. Genetics. 1993;134:
1177 869-893.

1178 42. Yukilevich R, True JR. African morphology, behavior, and phermones underlie
1179 incipient sexual isolation between US and Caribbean Drosophila melanogaster.
1180 Evolution. 2008;62: 2807–2828. doi:10.1111/j.1558-5646.2008.00488.x

1181 43. Lachance J, True JR. X-autosome incompatibilities in Drosophila melanogaster: test of
1182 Haldane's rue and geographic patterns within species. Evolution. 2010;64: 3035–
1183 3046. doi:10.1111/j.1558-5646.2010.01028.x

1184 44. Corbett-Detig RB, Zhou J, Clark AG, Hartl DL, Ayroles JF. Genetic incompatibilities are
1185 widespread within species. Nature. 2013;504: 135–137. doi:10.1038/nature12678

1186 45. Kofler R, Betancourt AJ, Schlotterer C. Sequencing of Pooled DNA Samples (Pool-Seq)
1187 Uncovers Complex Dynamics of Transposable Element Insertions in Drosophila
1188 melanogaster. PLoS Genet. 2012;8: e1002487–16.
1189 doi:10.1371/journal.pgen.1002487

1190 46. terWengel PO, Kapun M, Nolte V, Kofler R, Flatt T, Schlotterer C. Adaptation of
1191 *Drosophila* to a novel laboratory environment reveals temporally heterogeneous
1192 trajectories of selected alleles. Mol Ecol. 2012;21: 4931–4941. doi:10.1111/j.1365-
1193 294X.2012.05673.x

1194 47. Kolaczkowski B, Kern AD, Holloway AK, Begun DJ. Genomic differentiation between
1195 temperate and tropical Australian populations of Drosophila melanogaster. Genetics.
1196 2011;187: 245–260. doi:10.1534/genetics.110.123059

1197 48. Kapun M, Schalkwyk H, McAllister B, Flatt T, Schlotterer C. Inference of chromosomal
1198 inversion dynamics from Pool-Seq data in natural and laboratory populations of
1199 Drosophila melanogaster. Mol Ecol. 2014;23: 1813–1827. doi:10.1111/mec.12594

1200 49. Zhu Y, Bergland AO, González J, Petrov DA. Empirical validation of pooled whole
1201 genome population re-sequencing in Drosophila melanogaster. PLoS ONE. 2012;7:
1202 e41901. doi:10.1371/journal.pone.0041901

1203 50. Liang M, Nielsen R. The lengths of admixture tracts. Genetics. 2014;197: 953–967.

doi:10.1534/genetics.114.162362

51. Moltke I, Grarup N, Jørgensen ME, Bjerregaard P, Treebak JT, Fumagalli M, et al. A common Greenlandic TBC1D4 variant confers muscle insulin resistance and type 2 diabetes. Nature. 2014;512: 190–193. doi:10.1038/nature13425

52. Moltke I, Fumagalli M, Korneliussen TS. Uncovering the genetic history of the present-day Greenlandic population. Am J Hum Genet. 2015;96: 54–69. doi:10.1016/j.ajhg.2014.11.012

53. Voight BF, Kang HM, Ding J, Palmer CD, Sidore C, Chines PS, et al. The metabochip, a custom genotyping array for genetic studies of metabolic, cardiovascular, and anthropometric traits. PLoS Genet. 2012;8: e1002793–12. doi:10.1371/journal.pgen.1002793

54. Corbett-Detig RB, Hartl DL. Population genomics of inversion polymorphisms in Drosophila melanogaster. PLoS Genet. 2012;8: e1003056–15. doi:10.1371/journal.pgen.1003056

55. Kapun M, Fabian DK, Goudet J, Flatt T. Genomic evidence for adaptive inversion clines in Drosophila melanogaster. Mol Biol Evol. 2016;33: 1317–1336. doi:10.1093/molbev/msw016

56. Mackay TFC, Richards S, Stone EA, Barbadilla A, Ayroles JF, Zhu D, et al. The Drosophila melanogaster Genetic Reference Panel. Nature. 2012;482: 173–178. doi:10.1038/nature10811

1224 57. Huang W, Massouras A, Inoue Y, Peiffer J, Ramia M, Tarone AM, et al. Natural
1225 variation in genome architecture among 205 Drosophila melanogaster Genetic
1226 Reference Panel lines. Genome Res. 2014;24: 1193–1208.
1227 doi:10.1101/gr.171546.113

1228 58. Corbett-Detig RB, Cardeno C, Langley CH. Sequence-based detection and breakpoint
1229 assembly of polymorphic inversions. Genetics. 2012;192: 131–137.
1230 doi:10.1534/genetics.112.141622

1231 59. Kulathinal RJ, Stevison LS, Noor MAF. The genomics of speciation in Drosophila:
1232 diversity, divergence, and introgression estimated using low-coverage genome
1233 sequencing. PLoS Genet. 2009;5: e1000550–7. doi:10.1371/journal.pgen.1000550

1234 60. Krimbas CB, Powell JR. Drosophila Inversion Polymorphism. CRC Press; 1992.

1235 61. Aulard S, David JR, Lemenieur F. Chromosomal inversion polymorphism in
1236 Afrotropical populations of *Drosophila melanogaster*. Genet Res. 2002;79: 49–63.
1237 doi:10.1017/S0016672301005407

1238 62. Ting CT, Takahashi A, Wu CI. Incipient speciation by sexual isolation in Drosophila:
1239 concurrent evolution at multiple loci. PNAS. 2001;98: 6709–6713.

1240 63. Hollocher H, Ting CT, Wu ML, Wu CI. Incipient speciation by sexual isolation in
1241 Drosophila melanogaster: extensive genetic divergence without reinforcement.
1242 Genetics. 1997;147: 1191–1201.

1243 64. Hollocher H, Ting CT, Pollack F, Wu CI. Incipient speciation by sexual isolation in

1244 Drosophila melanogaster: variation in mating preference and correlation between
1245 sexes. Evolution. 1997;51: 1175–1181.

1246 65. Coyne JA. Genetics and speciation. Nature. 1992;335: 511–515.

1247 66. Coyne JA, Orr HA. Patterns of speciation in Drosophila. Evolution. 1989;43: 362–381.

1248 67. Charlesworth B, Coyne JA, Barton NH. The relative rates of evolution of sex
1249 chromosomes and autosomes. American Naturalist. 1987;130: 113–146.

1250 68. Ellis LL, Carney GE. Socially-Responsive Gene Expression in Male Drosophila
1251 melanogaster Is Influenced by the Sex of the Interacting Partner. Genetics. 2011;187:
1252 157–169. doi:10.1534/genetics.110.122754

1253 69. Edwards AC, Zwarts L, Yamamoto A, Callaerts P, Mackay TF. Mutations in many genes
1254 affect aggressive behavior in Drosophila melanogaster. BMC Biol. 2009;7: 29–13.
1255 doi:10.1186/1741-7007-7-29

1256 70. Nielsen R, Korneliussen T, Albrechtsen A, Li Y, Wang J. SNP calling, genotype calling,
1257 and sample allele frequency estimation from new-generation sequencing data. PLoS
1258 ONE. 2012;7: e37558–11. doi:10.1371/journal.pone.0037558

1259 71. Fumagalli M, Vieira FG, Linderoth T, Nielsen R. ngsTools: methods for population
1260 genetics analyses from next-generation sequencing data. Bioinformatics. 2014;30:
1261 1486–1487.

1262 72. DePristo MA, Banks E, Poplin R, Garimella KV, Maguire JR, Hartl C, et al. A framework
1263 for variation discovery and genotyping using next-generation DNA sequencing data.

1264 Nat Genet. 2011;43: 491–498. doi:10.1038/ng.806

1265 73. Baird SJE, Barton NH, Etheridge AM. The distribution of surviving blocks of an
1266 ancestral genome. Theoretical Population Biology. 2003;64: 451–471.
1267 doi:10.1016/S0040-5809(03)00098-4

1268 74. Henn BM, Botigué LR, Gravel S, Wang W, Brisbin A, Byrnes JK, et al. Genomic ancestry
1269 of north Africans supports back-to-Africa migrations. PLoS Genet. 2012;8:
1270 e1002397–11. doi:10.1371/journal.pgen.1002397

1271 75. Moorjani P, Patterson N, Hirschhorn JN, Keinan A, Hao L, Atzmon G, et al. The history
1272 of African gene flow into southern Europeans, Levantines, and Jews. PLoS Genet.
1273 2011;7: e1001373–13. doi:10.1371/journal.pgen.1001373

1274 76. Loh PR, Lipson M, Patterson N, Moorjani P. Inferring admixture histories of human
1275 populations using linkage disequilibrium. Genetics. 2013;193: 1233–1254.
1276 doi:10.1534/genetics.112.147330/-/DC1

1277 77. Marjoram P, Wall JD. Fast “coalecsent” simulation. BMC Genet. BioMed Central;
1278 2006;7: 16–9. doi:10.1186/1471-2156-7-16

1279 78. Kiefer J. Sequential minimax search for a maximum. Proceedings of the American
1280 Mathematical Society. 1953;4: 502–506.

1281 79. Chen GK, Marjoram P, Wall JD. Fast and flexible simulation of DNA sequence data.
1282 Genome Res. 2008;19: 136–142. doi:10.1101/gr.083634.108

1283 80. Gutenkunst RN, Hernandez RD, Williamson SH, Bustamante CD. Inferring the joint

1284 demographic history of multiple populations from multidimensional SNP frequency
1285 data. PLoS Genet. 2009;5: e1000695–11. doi:10.1371/journal.pgen.1000695

1286 81. Corbett-Detig R, Jones M. SELAM: Simulation of Epistasis and Local adaptation during
1287 Admixture with Mate choice. Bioinformatics. 2016;btw365.

1288 82. Pool JE, Aquadro CF. History and Structure of Sub-Saharan Populations of Drosophila
1289 melanogaster. Genetics. 2006;174: 915–929. doi:10.1534/genetics.106.058693

1290 83. Lack JB, Cardeno CM, Crepeau MW, Taylor W, Corbett-Detig RB, Stevens KA, et al. The
1291 Drosophila Genome Nexus: a population genomic resource of 623 Drosophila
1292 melanogaster genomes, including 197 from a single ancestral range population.
1293 Genetics. 2015;199: 1229–1241. doi:10.1534/genetics.115.174664/-/DC1

1294 84. Li H. Aligning sequence reads, clone sequences and assembly contigs with BWA-
1295 MEM. arXiv preprint arXiv:13033997. 2013.

1296 85. Adams MD, Celniker SE, Holt RA, Evans CA, Gocayne JD, Amanatides PG. The genome
1297 sequence of Drosophila melanogaster. Genetics. 2000;287: 2185–2195.

1298 86. Li H, Handsaker B, Wysoker A, Fennell T, Ruan J, Homer N, et al. The Sequence
1299 Alignment/Map format and SAMtools. Bioinformatics. 2009;25: 2078–2079.
1300 doi:10.1093/bioinformatics/btp352

1301 87. Comeron JM, Ratnappan R, Bailin S. The many landscapes of recombination in
1302 Drosophila melanogaster. PLoS Genet. 2012;8: e1002905.
1303 doi:10.1371/journal.pgen.1002905

1304 88. Best DJ, Roberts DE. Algorithm AS 89: the upper tail probabilities of Spearman's rho.
1305 Journal of the Royal Statistical Society Series C. 1975;24: 377–379.

1306 89. Kao JY, Lymer S, Hwang SH, Sung A, Nuzhdin SV. Postmating reproductive barriers
1307 contribute to the incipient sexual isolation of the United States and Caribbean
1308 Drosophila melanogaster. Ecol Evol. 2015;5: 3171–3182. doi:10.1002/ece3.1596

1309 90. Eden E, Navon R, Steinfeld I, Lipson D, Yakhini Z. GOrilla: a tool for discovery and
1310 visualization of enriched GO terms in ranked gene lists. BMC Bioinformatics 2013
1311 14:1. BioMed Central; 2009;10: 48–7. doi:10.1186/1471-2105-10-48

1312

1313

Figure 1. The effect of increasing stringency with ancestral LD pruning. From left to right, ancestry proportions are 0.1, 0.25, 0.5, 0.75 and 0.9. |r| cutoffs are: none (red), 1.0 (orange), 0.9 (yellow), 0.8 (green), 0.7 (dark blue), 0.6 (cyan), 0.5 (indigo), and 0.4 (violet). The solid line indicates the expectation for unbiased time estimation. All read data were simulated with ploidy = 1. True admixture time was drawn from a uniform (0, 2000) distribution.

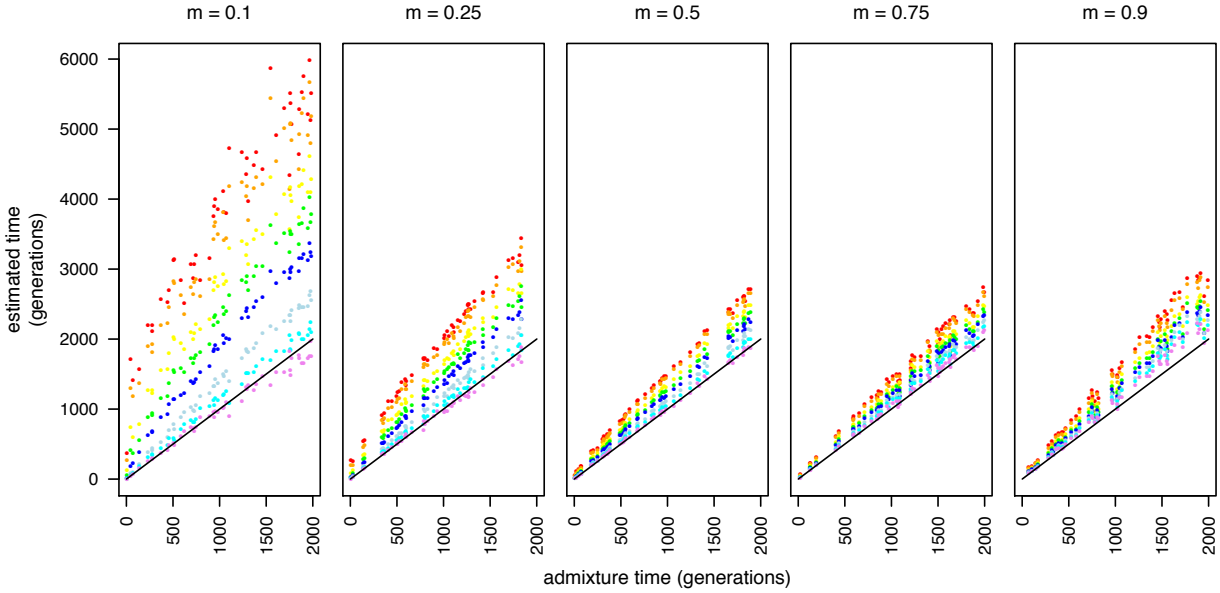

Figure 2. Time estimates and accuracy statistics for samples of varying ploidies. From left to right, ancestry proportions are 0.1, 0.25, 0.5, 0.75 and 0.9. Each sample ploidy is represented by one point color with ploidy one (black), two (red), ten (blue) and twenty (green). From top to bottom, each row is the estimated time in generations, the proportion of sites where the true state is within the 95% credible interval, the width of the 95% credible interval, the mean posterior error, and the proportion of sites where the maximum likelihood estimate is equal to the true state.

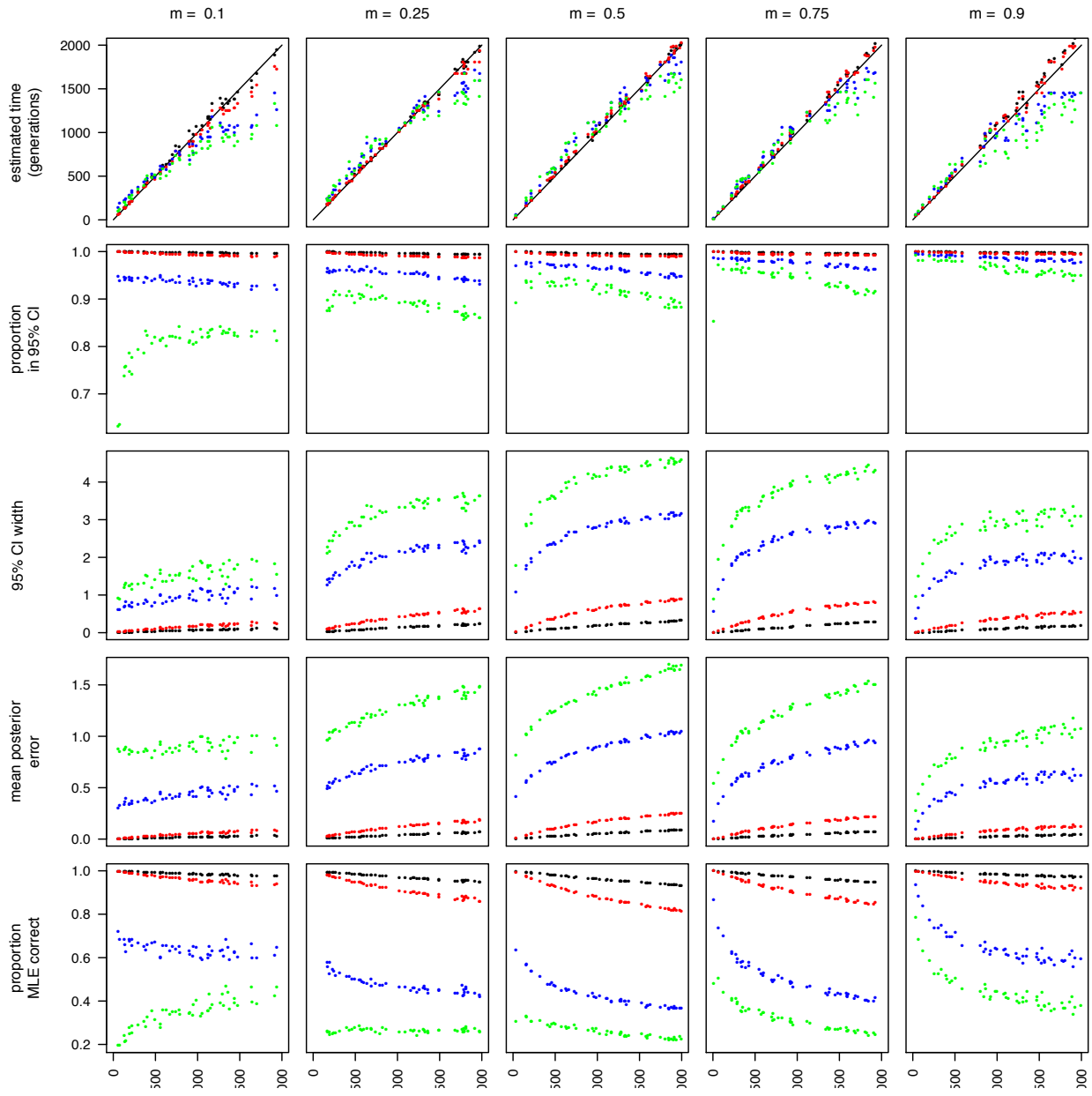

1335 **Figure 3.** Comparison between LAI using the full ancestral recombination graph via
1336 forward-time simulations (red) with those from independent and identically distributed
1337 draws from the SMC' distribution (black). Simulations were conducted using an ancestry
1338 proportion of 0.25 and population size of 10,000 hermaphroditic individuals.

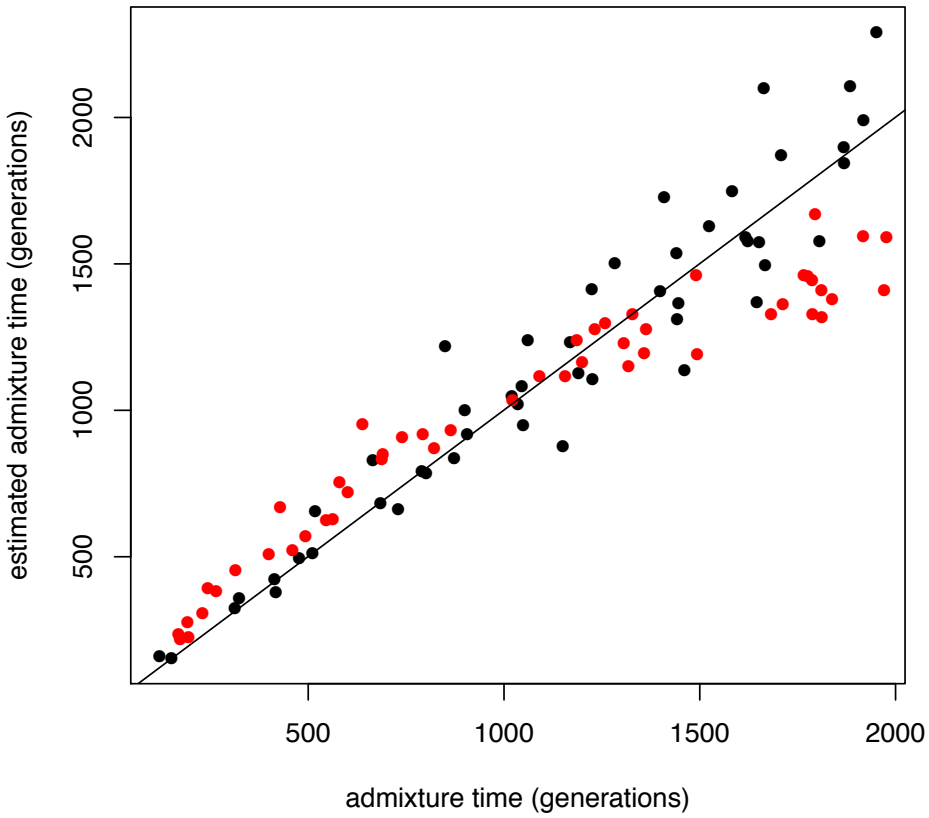

1339
1340

Figure 4. Effects of unknown admixed population sizes on LAI. All LAI was conducted assuming the true population size was 10,000. Simulated population sizes were 100 (black), 1,000 (red), 10,000 (blue) and 100,000 (green). Ploidy 1 on the right, ploidy 2 on the left. From top to bottom, rows are the estimated time of admixture, the proportion of sites where the true state is within the 95% credible interval, the width of the 95% credible interval, the mean posterior error, and the proportion of times that the maximum likelihood estimate is equal to the true state. For all simulations, the ancestry proportion was equal to 0.5.

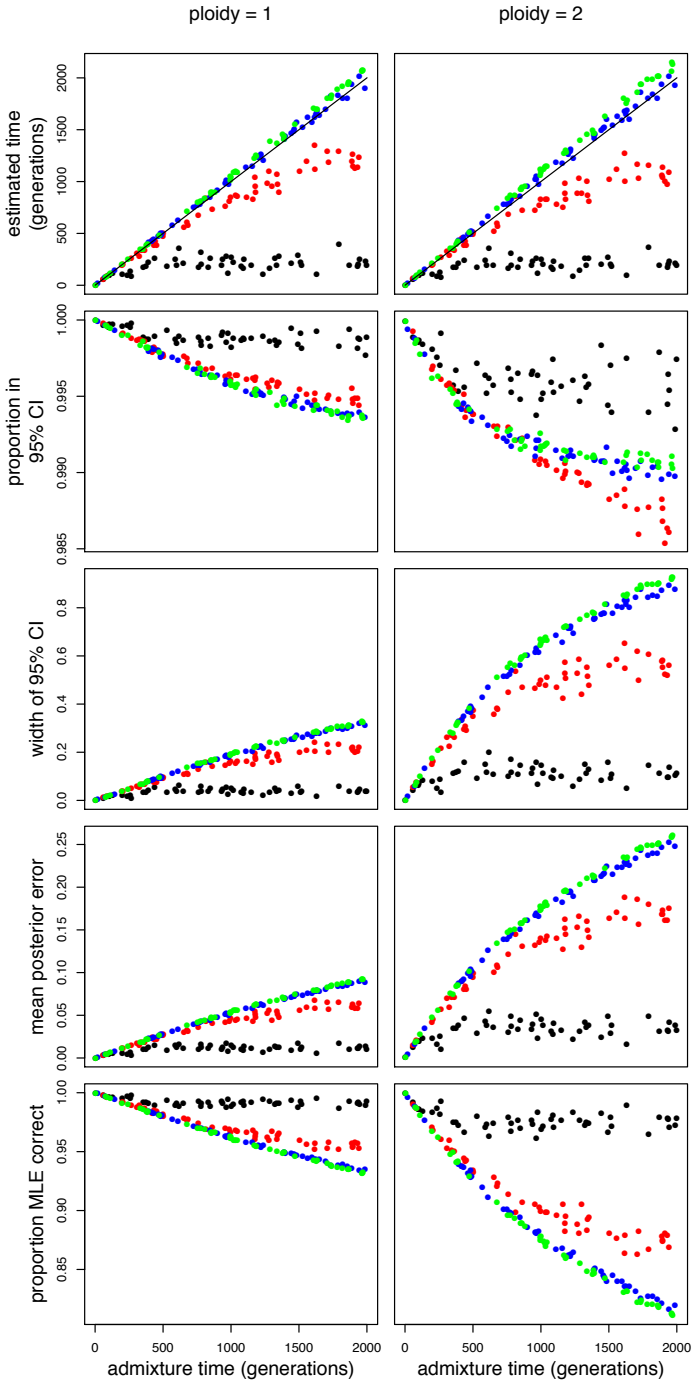

Figure 5. LAI accuracy when admixture times are increasingly ancient. Here, ancestry proportions are 0.5 (black), 0.25 (blue), 0.1 (violet), 0.75 (orange) and 0.9 (red). From top to bottom, statistics plotted are estimated time, the proportion of sites where the true ancestry frequency is within the 95% credible interval, the mean 95% credible interval width, mean posterior error, and the proportion of times that the maximum likelihood estimate is correct.

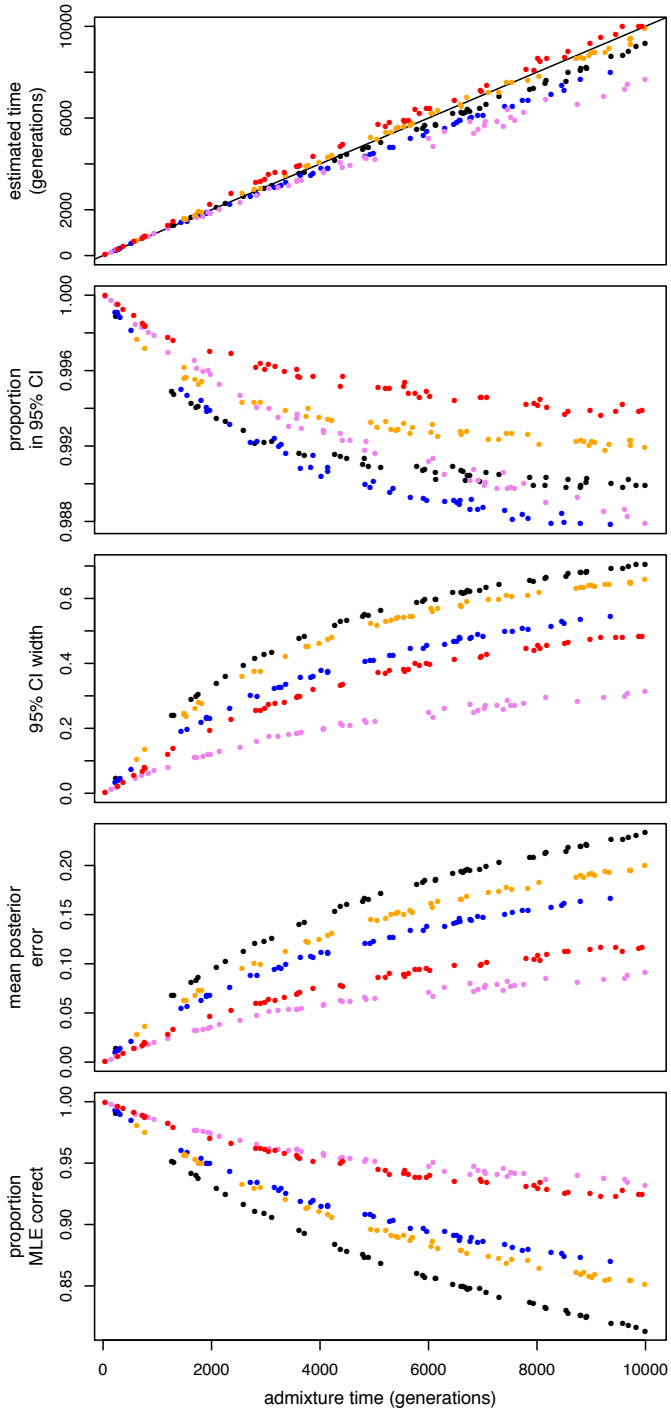

Figure 6. The effects of reference panel size on LAI and time estimation using the HMM. Here, we compare reference panels of size 100 (blue) with reference panels of size 10 (black). From left to right, ancestry proportions are 0.1, 0.25, 0.5, 0.75 and 0.9. From top to bottom the plotted statistics are estimated time, proportion in the 95% credible interval, the average width of the 95% credible interval, the mean posterior error, and the proportion of sites where the maximum likelihood ancestry estimate is correct.

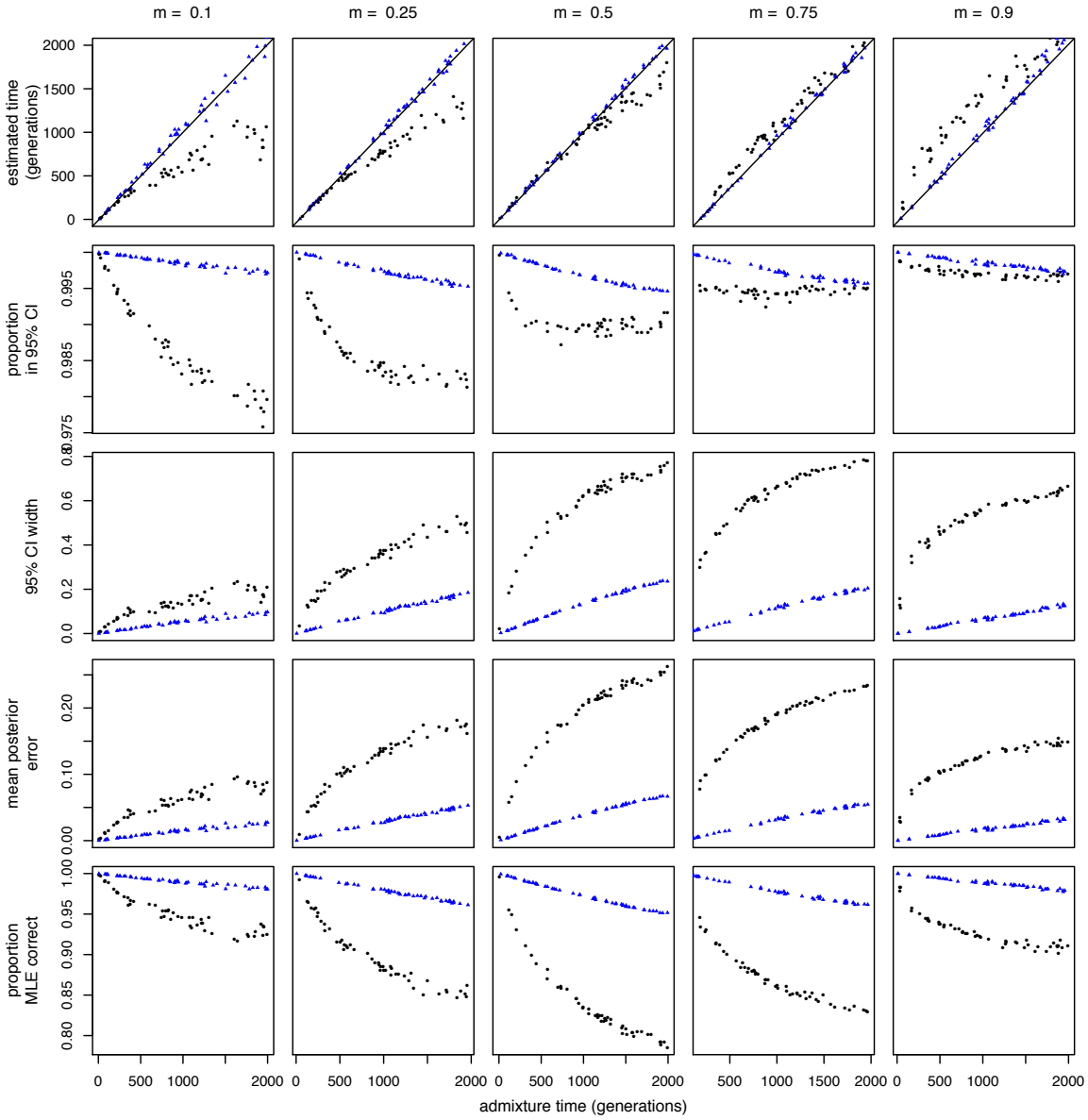

Figure 7. Accuracy of the HMM for samples of high ploidy. The 95% credible interval (shaded blue region), and the posterior mean (red) contrasted with the true ancestry frequencies (black). Simulated data were generated with an admixture time of 1500 generations, an ancestry proportion of 0.2, a sample ploidy of 100, and a mean sequencing depth of 25.

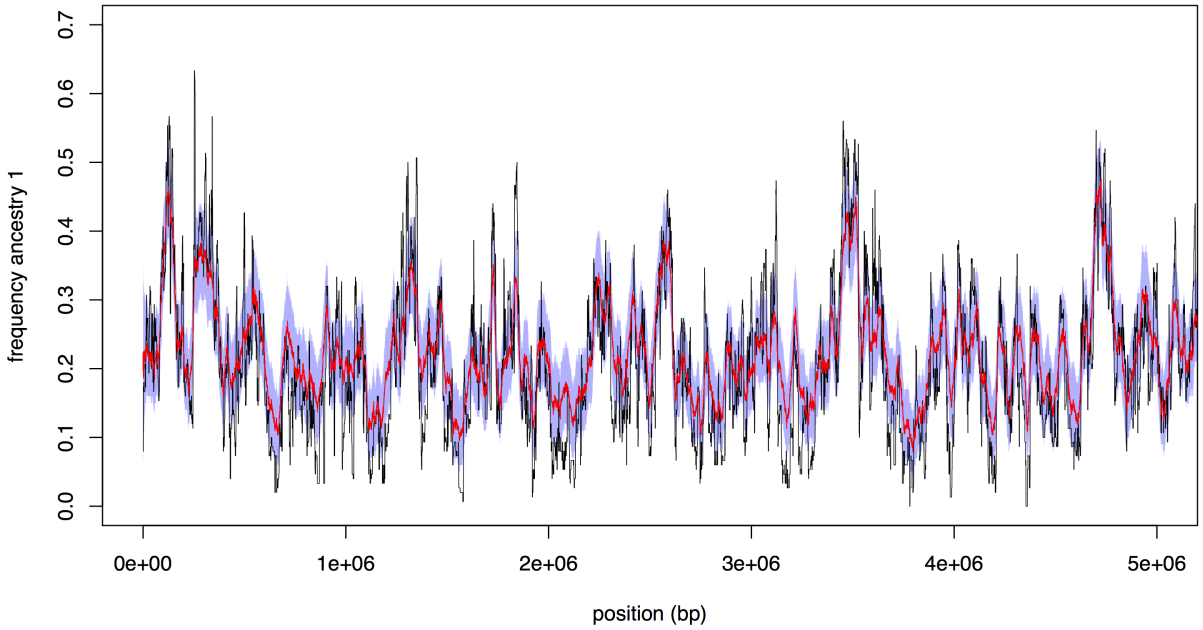

Figure 8. Comparison of the proportion of sites where the maximum likelihood ancestry estimate of local ancestry is correct between LAMPanc and our method. LAMPanc was run with default parameters (black), and with LD pruned in the ancestral populations, but not in the admixed population (red). Our method was run with default parameters (blue), but with the time since admixture and correct ancestry proportion supplied to our program as these parameters are required by LAMPanc.

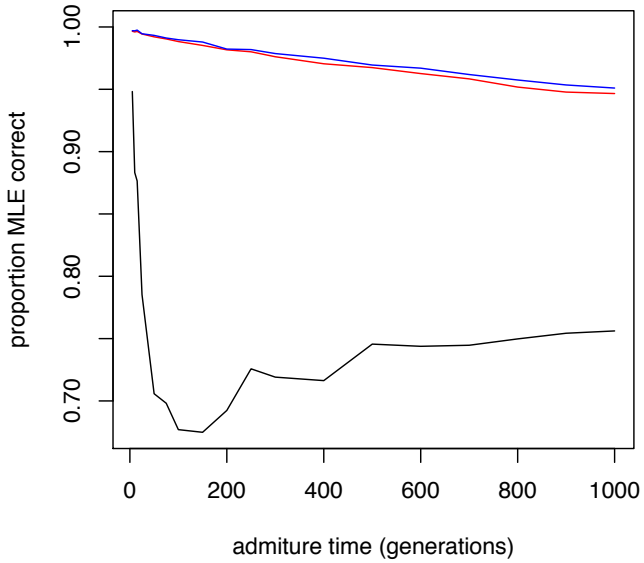

Figure 9. Admixture time estimates for simulated data consistent with variation present in modern European and African populations. From left to right, m = 0.1, m = 0.25, m = 0.5, m = 0.75, m = 0.9. Top row is completely phased chromosomes and the bottom row is for unphased diploid data.

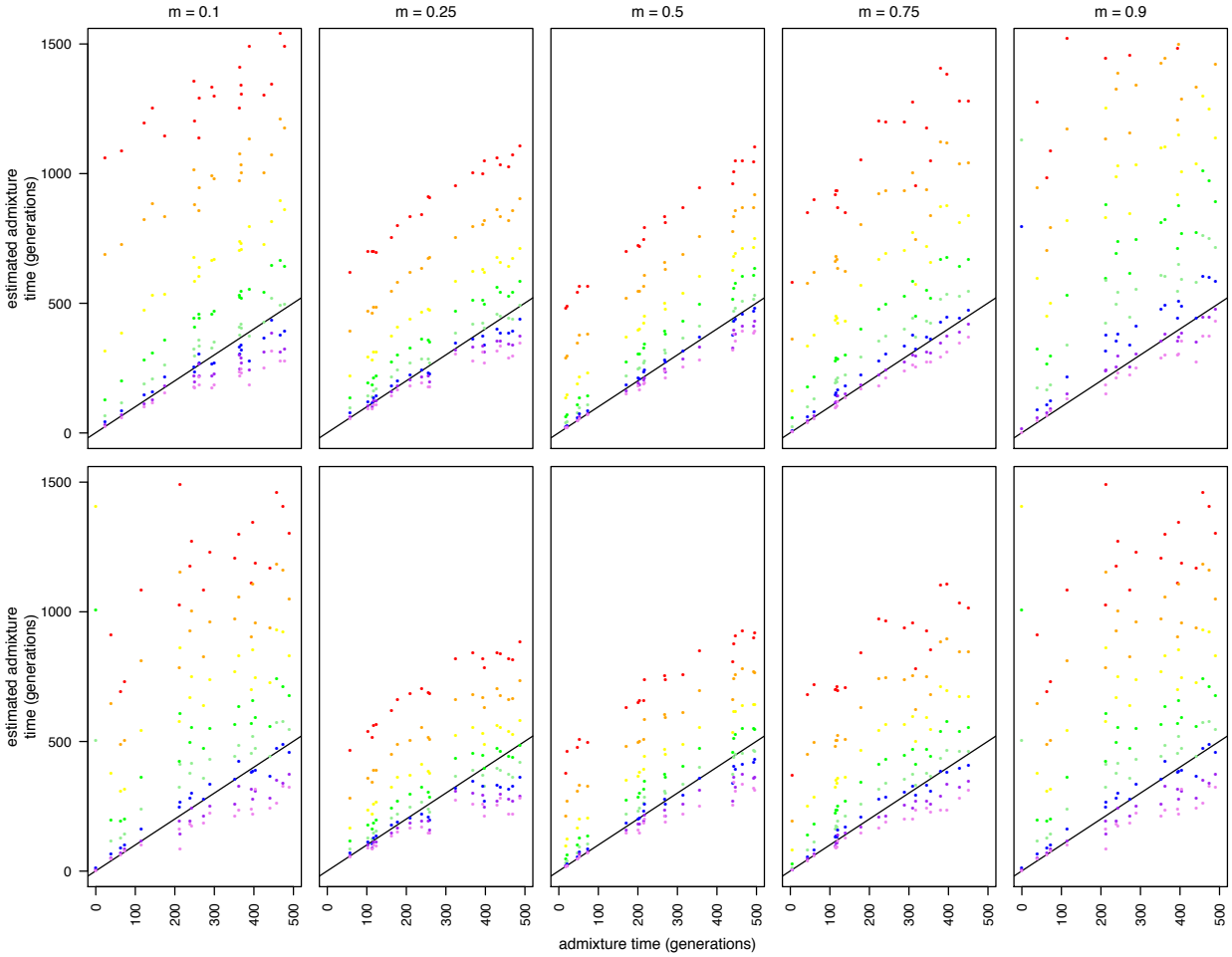

Figure 10. Bias in LAI due to uncertainty in *t*. The posterior probability of European ancestry at a given site in the genome assuming t = 5 (black) and assuming t = 20 (red) for a sample representative of the average difference (top left) and a more extreme example (top right). The distribution of differences in mean Inuit ancestry for all samples (bottom left). The log likelihood of each time since admixture as computed using our method (bottom right), which shows a clear optimum at 6-7 generations since admixture. All analyses were restricted to SNPs on chromosome 10.

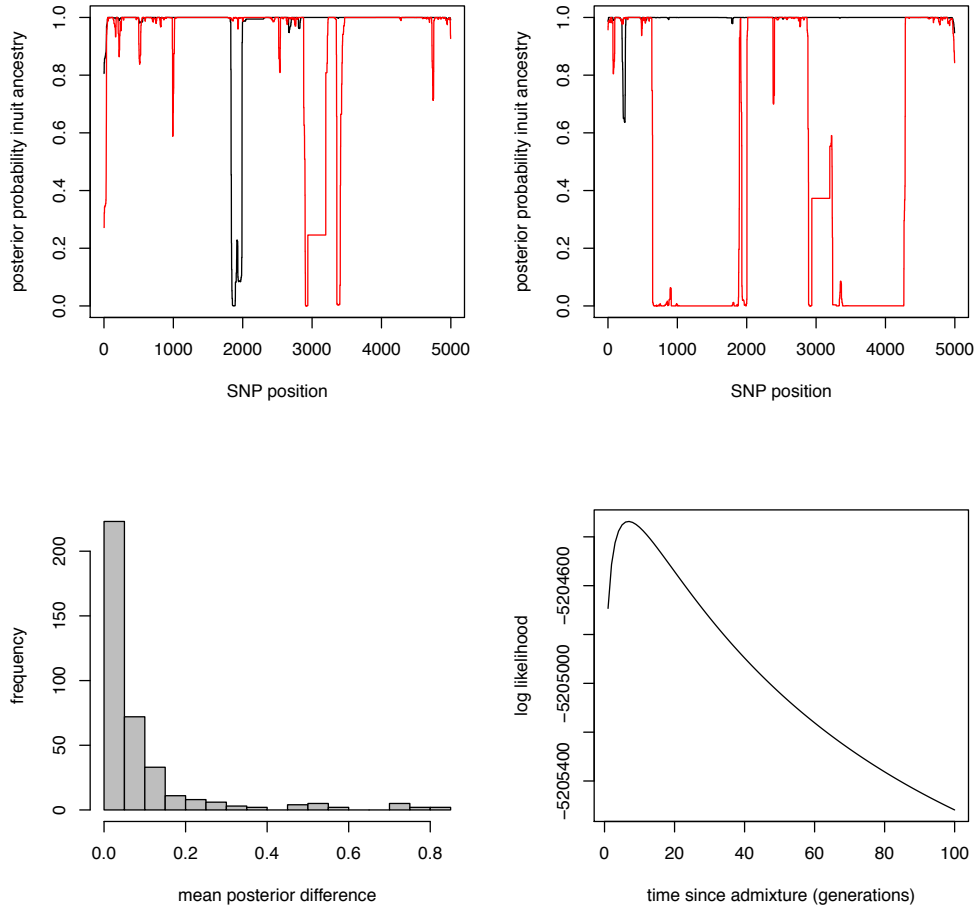

Figure 11. Local ancestry of inversion bearing chromosomes (red) compared with those of standard arrangement chromosomes (black) for the same chromosome arm. Positions of inversion breakpoints, as reported in {CorbettDetig:2012bq} are shown as vertical dashed lines.

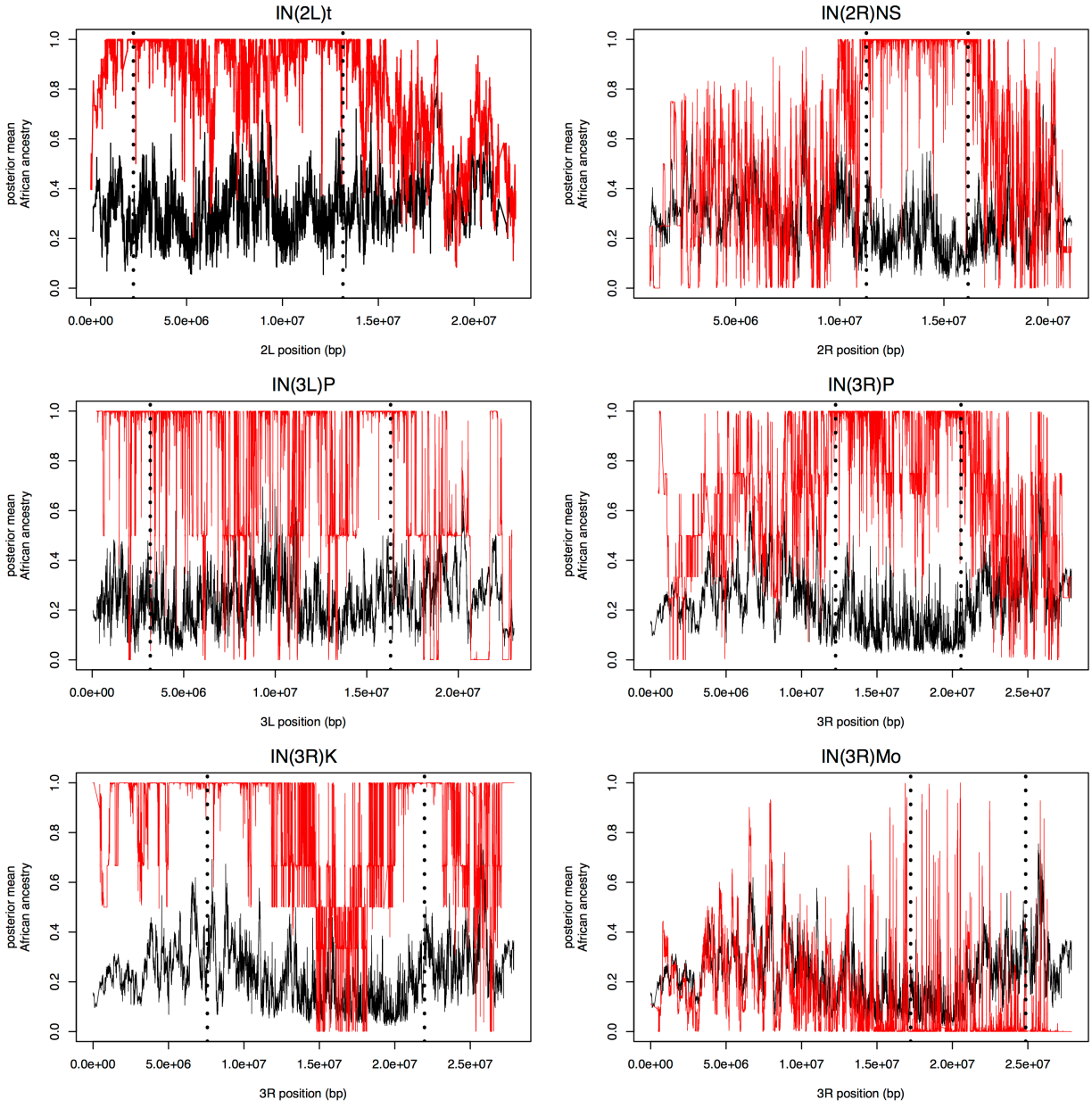

Figure 12. The partial correlation between LA and latitude with correction for chromosome-wide ancestry proportions. Sites for which the probability of the observed clinal relationship was less than 0.005 were retained as significant (red). Inversion breakpoints for inversions that are at polymorphic frequencies on this ancestry cline are shown as dotted blue lines.